cmgh
CELLULAR AND MOLECULAR GASTROENTEROLOGY AND HEPATOLOGY

ORIGINAL RESEARCH

Wnt-induced, TRP53-mediated Cell Cycle Arrest of Precursors Underlies Interstitial Cell of Cajal Depletion During Aging

Yujiro Hayashi,[1,2] David T. Asuzu,[1,2] Michael R. Bardsley,[1,2] Gabriella B. Gajdos,[1,2] Sergiy M. Kvasha,[1,2] David R. Linden,[1] Rea A. Nagy,[1,2] Siva Arumugam Saravanaperumal,[1,2] Sabriya A. Syed,[1,2] Yoshitaka Toyomasu,[1,2] Huihuang Yan,[3] Eduardo N. Chini,[4] Simon J. Gibbons,[1] Todd A. Kellogg,[5] Khashayarsha Khazaie,[6] Makoto Kuro-o,[7,8] Jair Machado Espindola Netto,[4] Mahendra Pal Singh,[6] James G. Tidball,[9] Michelle Wehling-Henricks,[9] Gianrico Farrugia,[1] and Tamas Ordog[1,2,10]

[1]Enteric Neuroscience Program and Department of Physiology and Biomedical Engineering, Mayo Clinic, Rochester, Minnesota; [2]Gastroenterology Research Unit, Division of Gastroenterology and Hepatology, Department of Medicine, Mayo Clinic, Rochester, Minnesota; [3]Division of Biomedical Statistics and Informatics, Department of Health Sciences Research, Mayo Clinic, Rochester, Minnesota; [4]Signal Transduction and Molecular Nutrition Laboratory, Kogod Aging Center and Department of Anesthesiology and Perioperative Medicine, Mayo Clinic, Rochester, Minnesota; [5]Department of Surgery, Mayo Clinic, Rochester, Minnesota; [6]Department of Immunology, Mayo Clinic, Rochester, Minnesota; [7]Department of Internal Medicine, University of Texas Southwestern Medical Center, Dallas, Texas; [8]Division of Anti-aging Medicine, Center for Molecular Medicine, Jichi Medical University, Shimotsuke, Tochigi, Japan; [9]Department of Integrative Biology and Physiology, University of California, Los Angeles, California; and [10]Center for Individualized Medicine, Mayo Clinic, Rochester, Minnesota

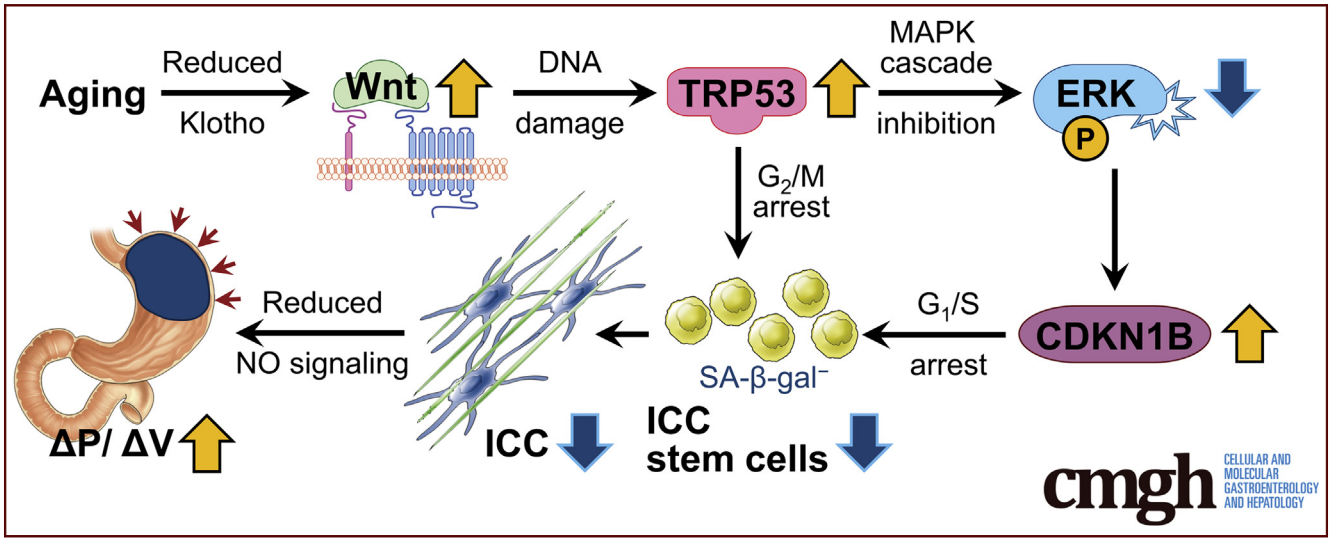

SUMMARY

Aging-associated depletion of interstitial cells of Cajal arises from persistent cell cycle arrest of precursors occurring without an increase in canonical senescence markers or apoptosis. The blockade of precursor self-renewal is initiated by unopposed Wnt signaling and mediated by TRP53.

BACKGROUND & AIMS: Gastric dysfunction in the elderly may cause reduced food intake, frailty, and increased mortality. The pacemaker and neuromodulator cells interstitial cells of Cajal (ICC) decline with age in humans, and their loss contributes to gastric dysfunction in progeric *klotho* mice hypomorphic for the anti-aging Klotho protein. The mechanisms of ICC depletion remain unclear. Klotho attenuates Wnt (wingless-type MMTV integration site) signaling. Here, we examined whether unopposed Wnt signaling could underlie aging-associated ICC loss by up-regulating transformation related protein TRP53 in ICC stem cells (ICC-SC).

METHODS: Mice aged 1–107 weeks, *klotho* mice, APC$^{\Delta 468}$ mice with overactive Wnt signaling, mouse ICC-SC, and human gastric smooth muscles were studied by RNA sequencing, reverse transcription–polymerase chain reaction, immunoblots, immunofluorescence, histochemistry, flow cytometry, and methyltetrazolium, ethynyl/bromodeoxyuridine incorporation, and ex-vivo gastric compliance assays. Cells were manipulated pharmacologically and by gene overexpression and RNA interference.

RESULTS: The *klotho* and aged mice showed similar ICC loss and impaired gastric compliance. ICC-SC decline preceded ICC

depletion. Canonical Wnt signaling and TRP53 increased in gastric muscles of *klotho* and aged mice and middle-aged humans. Overstimulated canonical Wnt signaling increased DNA damage response and TRP53 and reduced ICC-SC self-renewal and gastric ICC. TRP53 induction persistently inhibited G_1/S and G_2/M cell cycle phase transitions without activating apoptosis, autophagy, cellular quiescence, or canonical markers/mediators of senescence. G_1/S block reflected increased cyclin-dependent kinase inhibitor 1B and reduced cyclin D1 from reduced extracellular signal-regulated kinase activity.

CONCLUSIONS: Increased Wnt signaling causes age-related ICC loss by up-regulating TRP53, which induces persistent ICC-SC cell cycle arrest without up-regulating canonical senescence markers. *(Cell Mol Gastroenterol Hepatol 2021;11:117–145; https://doi.org/10.1016/j.jcmgh.2020.07.011)*

Keywords: Stem Cell; Senescence; Compliance.

Aging is associated with a progressive decline in the functions of most organs including of the gastrointestinal tract.[1] Age-related gastrointestinal dysfunctions include gastroesophageal reflux, silent aspiration, postprandial hypotension, irritable bowel syndrome, constipation, and fecal incontinence.[2,3] Although reports of altered gastric emptying have been inconsistent,[4] reduced fundal compliance and accommodation leading to prolonged antral distention may contribute to early satiety and increased satiation in the elderly.[3–5] Indeed, body weight decreases steadily by an average of 0.5% per year when older than 65 years of age, reflecting a decline in food intake termed *anorexia of aging*.[3] Reduced protein intake accompanying this weight loss has been linked to increased cancer and overall mortality,[6] underscoring the need for a better understanding of the mechanisms of age-related gastric dysfunctions.

Impaired gastric compliance and accommodation could reflect loss of nitrergic neurons or their function.[7] However, age-related depletion of enteric neurons is less evident in the stomach, and nitrergic neurons are spared in aging humans, rats, and mice.[8–13] In contrast, interstitial cells of Cajal (ICC), electrical pacemakers, mediators of nitrergic and cholinergic neuromuscular neurotransmission, and regulators of smooth muscle membrane potential and tone,[14] steadily decline at a rate of ∼13% per decade of adult life.[15] In progeric mice hypomorphic for the anti-aging protein Klotho (*klotho* mice),[16] we previously reported a profound decrease in gastric ICC accompanying impaired fundal nitrergic inhibitory neuromuscular neurotransmission, which occurred without a reduction in neuronal nitric oxide synthase expression or enteric neuron numbers.[11] Therefore, ICC loss may be central to age-related gastric dysfunction.

Cellular senescence is an irreversible state of cell growth arrest induced by cellular stress and an important driver of aging and age-related diseases.[17,18] Stem cell senescence plays a key part in organ dysfunctions during aging.[19] Indeed, we previously reported depletion of ICC stem cells (ICC-SC)[20–22] in the stomach of *klotho* mice,[11] suggesting that senescence or other mechanisms affecting these ICC precursors may be important for age-related ICC loss.

Whereas the wingless-type MMTV integration site (Wnt) pathway is critical for stem cell homeostasis,[23,24] overactive Wnt signaling can lead to cancer or cellular senescence[25–27] as shown in stem cells residing in various tissues of *klotho* mice.[28] Wnt-induced senescence may involve stabilization of transformation related protein 53 (TRP53),[29] a multifunctional protein with well-established roles in DNA damage response (DDR), apoptosis, metabolism, autophagy, cell cycle inhibition/arrest, cellular senescence, aging, and cancer.[17,18,30–33] A similar mechanism may also affect ICC-SC. However, the function of Wnt signaling in the ICC lineage has not been characterized. Here, we investigated the hypothesis that aberrant activation of Wnt signaling leads to ICC depletion by triggering ICC-SC senescence via TRP53 up-regulation. Our findings in cultured ICC-SC, progeric *klotho* and naturally aged mice, in $APC^{\Delta 468}$ mice with genetic up-regulation of canonical Wnt signaling,[34] and in human gastric tissues obtained from young and middle-aged donors identify a novel role for canonical Wnt signaling in ICC-SC proliferation and establish a link between overactive Wnt and TRP53 signaling and ICC-SC/ICC aging. Our data also reveal a role for TRP53-induced persistent cell cycle arrest occurring without apoptosis, autophagy, cellular quiescence, or the up-regulation of canonical mediators of senescence in aging-associated ICC-SC dysfunction.

Results

Aging-related Interstitial Cell of Cajal and Interstitial Cell of Cajal Stem Cell Decline Is Associated With Impaired Gastric Compliance

Gastric ICC decline in humans with age,[15] and both ICC and ICC-SC are robustly reduced in progeric *klotho* mice, leading to impaired nitrergic inhibitory neuromuscular

Abbreviations used in this paper: **ANO1, anoctamin-1; ANOVA, analysis of variance; APC, allophycocyanin; BrdU, 5-bromo-2′-deoxyuridine; CCND1, cyclin D1; CDKN1A, cyclin-dependent kinase inhibitor 1a; CDKN1B, cyclin-dependent kinase inhibitor 2B; CL.CASP3, cleaved caspase 3; CTNNB1, catenin beta 1; DAPI, 4′,6-diamidino-2-phenylindole; DDR, DNA damage response; DMSO, dimethyl sulfoxide; EdU, 5-ethynyl-2′-deoxyuridine; ERK, extracellular signal-regulated kinase; ETV1, ets variant 1; FDR Q, false discovery rate Q value; GAPDH, glyceraldehyde-3-phosphate dehydrogenase; GEO, Gene Expression Omnibus; GSEA, gene set enrichment analysis; ICC, interstitial cells of Cajal; ICC-SC, interstitial cells of Cajal stem cells; KIT, v-kit Hardy-Zuckerman 4 feline sarcoma viral oncogene homolog; KLF4, Kruppel-like factor 4; MEK, mitogen-activated protein kinase kinase; MTS, methyltetrazolium salt; MYC, myelocytomatosis oncogene; NES, normalized enrichment score; PE, R-phycoerythrin; PI, propidium iodide; RNA-seq, RNA sequencing; RPKM, reads per kilobase of transcript per million mapped reads; RT-qPCR, real-time quantitative reverse-transcription polymerase chain reaction; SA-β-gal, senescence-associated beta-galactosidase; SESN, sestrin; siRNA, small interfering RNA; TRP53, transformation related protein 53; tsTAg, tsA58-mutant SV40 large T antigen; WB, Western immunoblotting; WT, wild-type.**

Most current article

2352-345X
https://doi.org/10.1016/j.jcmgh.2020.07.011

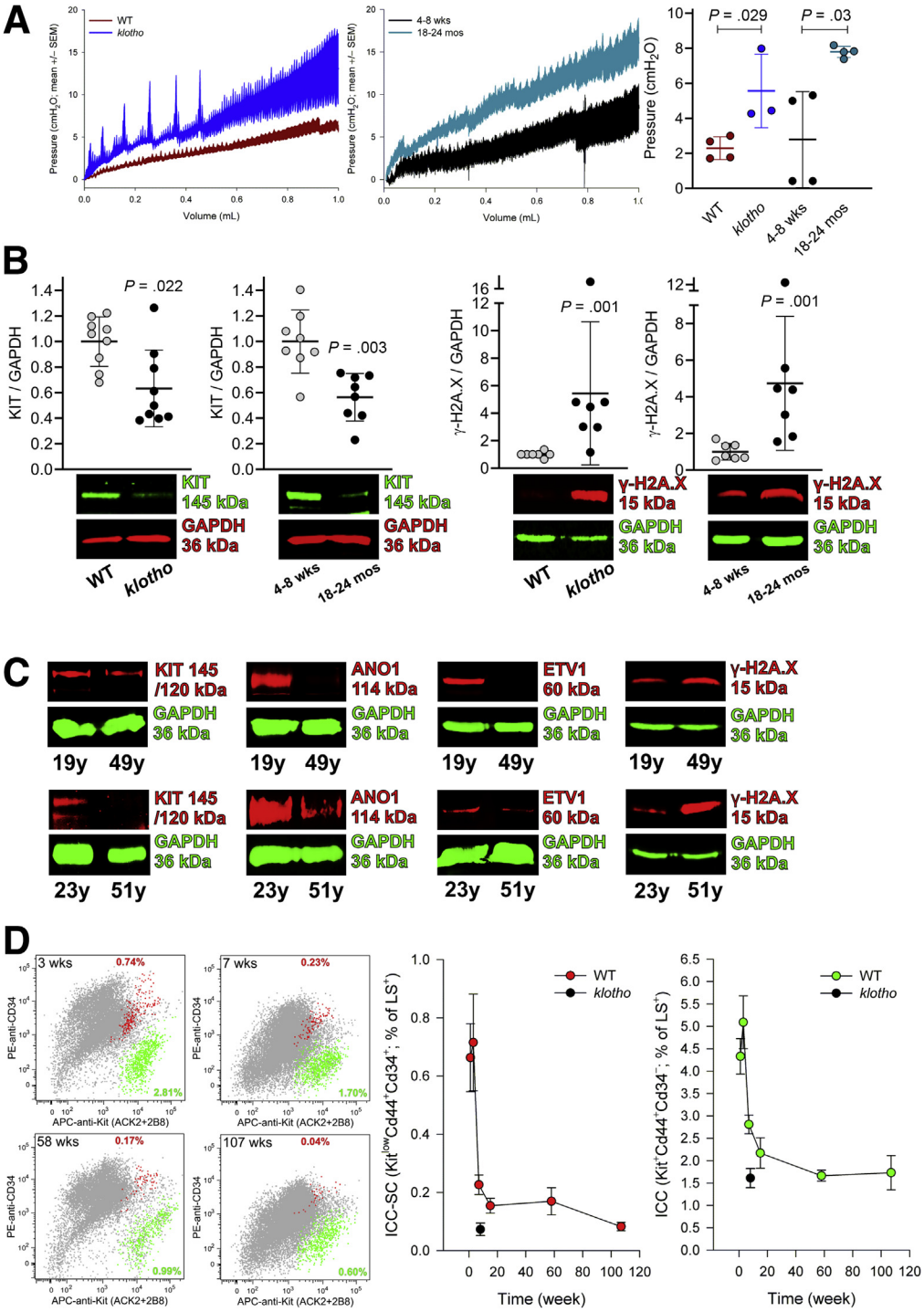

Figure 1. Age-related ICC and ICC-SC decline is associated with impaired gastric compliance. (*A*) Reduced gastric compliance of intact stomachs excised from 3 50- to 70-day-old *klotho* and 4 18- to 24-month-old C57BL/6 mice relative to age-matched WT (n = 4) and 4- to 8-week-old controls (n = 4), respectively (average traces). Stomachs were infused with 1 mL Krebs solution[36] at 37°C at a rate of 0.1 mL/min while recording luminal pressure. *P* values are from Mann-Whitney rank sum tests. (*B*) Reduced KIT protein and increased γ-H2A.X (H2AXS139p) protein in the gastric tunica muscularis of *klotho* vs WT mice (n = 5–9) and old (18–24 months) vs young (4–8 weeks) mice (n = 7–9/group). GAPDH was used as a loading control. *P* values are from Mann-Whitney rank sum tests. (*C*) Down-regulated ICC-related proteins (KIT, ANO1, ETV1) and up-regulated γ-H2A.X in gastric corpus muscles of 49-year-old male patient and 51-year-old female patient vs 19-year-old male and 23-year-old female controls. (*D*) Gastric ICC (KIT^+CD34^- subpopulation; *green*) and ICC-SC ($KIT^{low}CD34^+$ subpopulation; *red*) frequencies assessed by flow cytometry in a mixture of male and female C57BL/6 (n = 31) and BALB/c (n = 20) mice between 1 and 107 weeks of age (6–14 mice/time point). Representative projections (*left*) and time course data (*right*) depicting age-associated reduction in ICC and ICC-SC frequencies are shown. Data points in *black* are ICC and ICC-SC frequencies in 7- to 10-week-old *klotho* mice shown for comparison.[11]

Table 1. Representation of the "Signal Transduction_WNT Signaling" Network (Metacore) in Mouse Gastric ICC-SC, Mouse Small Intestinal and Colonic ICC, and Human Gastric ICC

Cells[a]	Species	Organ	Platform[b]	Data source	Analyzed data[c]	Cutoff[c]	Rank[d]	*P*[e]	FDR[e]	Ratio[f]	
										Genes in set	Genes in network
2xSCS2F10 (n = 2)	Mouse	Gastric corpus + antrum	HiSeq 2000 mRNA-seq	GSE60853[g]	Expression value	RPKM >0	23	1.35E-08	9.33E-08	163	177
2xSCS70 (n = 2)	Mouse	Gastric corpus + antrum	HiSeq 2000 mRNA-seq	GSE60853[g]	Expression value	RPKM >0	22	1.94E-08	1.40E-07	163	177
ICC (n = 1)	Mouse	Colon	HiSeq 2000 total RNA-seq	GSE57776	Expression value	RPKM >0	22	1.02E-07	7.34E-07	171	177
ICC (n = 1)	Mouse	Jejunum	HiSeq 2000 total RNA-seq	GSE57776	Expression value	RPKM >0	29	1.11E-06	6.10E-06	170	177
2xSCS2F10 (n = 3)	Mouse	Gastric corpus + antrum	MG430.2 Array	GSE60744[g]	DGE vs source tissue	Q <0.05 AND log_2FC >1	3	1.34E-11	7.05E-10	96	177
ICC-DMP (n = 3)	Mouse	Small intestines	MG430.2 Array	GSE7809	DGE vs source tissue	Q <0.05 AND log_2FC >1	4	3.17E-07	1.25E-05	38	177
ICC-MY (n = 3)	Mouse	Small intestines	MG430.2 Array	GSE7809	DGE vs source tissue	Q <0.05 AND log_2FC >1	5	2.98E-05	9.35E-04	30	177
2xSCS70 (n = 3)	Mouse	Gastric corpus + antrum	MG430.2 Array	GSE60744[g]	DGE vs source tissue	Q <0.05 AND log_2FC >1	39	8.21E-04	3.30E-03	46	177
ICC (n = 6)	Human	Gastric corpus + antrum	HGU133+2 Array	GSE77839	DGE vs source tissue	Q <0.05 AND log_2FC >1	20	2.32E-03	1.84E-02	103	177

[a]Cell lines: mouse gastric ICC-SC lines 2xSCS2F10 (C57BL/6) and 2xSCS70 (Immortomouse)[21,22]; FACS-purified native cells: colonic and jejunal ICC from *Kit*$^{+/copGFP}$ mice (background: 129S6Sv/Ev-C57BL/6J),[38] BALB/c mouse small intestinal ICC associated with the deep muscular plexus (ICC-DMP) and the myenteric plexus (ICC-MY),[39] and human gastric ICC.[40]
[b]Analysis platforms included mRNA- and total RNA-sequencing (Illumina HiSeq 2000), as well as Affymetrix Mouse Genome 430 2.0 Arrays (MG430.2) and Affymetrix Human Genome U133 Plus 2.0 Arrays (HGU133+2).
[c,d]RNA-seq data subjected to network analysis were normalized expression values (RPKM). Microarray data subjected to MetaCore network analysis were log_2 fold changes (FC) and false discovery rates (FDR, Benjamini-Hochberg *Q* values) from differential gene expression analysis (DGE) vs unfractionated tunica muscularis source tissues as follows: 2xSCS2F10 cells (n = 3) vs C57BL/6J gastric corpus + antrum (n = 2), 2xSCS70 cells (n = 3) vs Immortomouse gastric corpus + antrum (n = 3), ICC-DMP (n =3) and ICC-MY (n = 3) vs BALB/c small intestines (n = 2), and human ICC (n = 6) vs human gastric corpus + antrum (n = 4).
[d]Ranking of the Signal transduction_WNT signaling network among biological process networks detected by MetaCore analysis of gene sets meeting the specified cutoffs. See top 50 process networks for each cell type in Supplementary Datasets 1.
[e]*P* values and FDR *Q* values from the network analysis.
[f]Ratio of genes meeting cutoff criteria and all genes in the Signal transduction_WNT signaling network.
[g]Part of SuperSeries GSE60854.

Table 2. WNT Signaling-related Gene Sets Enriched in Mouse Gastric ICC-SC by Gene Set Enrichment Analysis

Gene set	2xSCS2F10 (m, ca, RS)			D2211B (m, ca, RS)			2xSCS70 (m, ca, RS)		
	Size	NES	FDR *Q*	Size	NES	FDR *Q*	Size	NES	FDR *Q*
BIOCARTA_WNT_PATHWAY	25[a]	2.33[a]	0.0011[a]	22[a]	1.54[a]	0.0885[a]	25[a]	2.24[a]	0.0021[a]
FEVR_CTNNB1_TARGETS_DN	491[a]	8.79[a]	0.0000[a]	467[a]	5.52[a]	0.0000[a]	486[a]	10.49[a]	0.0000[a]
FEVR_CTNNB1_TARGETS_UP	544[a]	3.53[a]	0.0000[a]	446[a]	3.31[a]	0.0000[a]	551[a]	2.62[a]	0.0004[a]
GO_CANONICAL_WNT_SIGNALING_PATHWAY	82[a]	1.68[a]	0.0383[a]	67	0.84	0.7592	82[a]	2.12[a]	0.0034[a]
GO_NEGATIVE_REGULATION_OF_CANONICAL_WNT_SIGNALING_PATHWAY	151[a]	4.02[a]	0.0000[a]	124[a]	3.58[a]	0.0000[a]	147[a]	3.70[a]	0.0000[a]
GO_NEGATIVE_REGULATION_OF_WNT_SIGNALING_PATHWAY	181[a]	3.99[a]	0.0000[a]	149[a]	3.56[a]	0.0000[a]	178[a]	3.34[a]	0.0000[a]
GO_NON_CANONICAL_WNT_SIGNALING_PATHWAY	134[a]	4.18[a]	0.0000[a]	117[a]	3.62[a]	0.0000[a]	136[a]	4.23[a]	0.0000[a]
GO_POSITIVE_REGULATION_OF_CANONICAL_WNT_SIGNALING_PATHWAY	113[a]	4.68[a]	0.0000[a]	102[a]	4.03[a]	0.0000[a]	114[a]	4.84[a]	0.0000[a]
GO_POSITIVE_REGULATION_OF_WNT_SIGNALING_PATHWAY	144[a]	4.71[a]	0.0000[a]	125[a]	4.05[a]	0.0000[a]	144[a]	4.54[a]	0.0000[a]
GO_REGULATION_OF_CANONICAL_WNT_SIGNALING_PATHWAY	218[a]	4.37[a]	0.0000[a]	180[a]	3.63[a]	0.0000[a]	214[a]	4.15[a]	0.0000[a]
GO_REGULATION_OF_NON_CANONICAL_WNT_SIGNALING_PATHWAY	18	1.00	0.4771	15	0.68	0.8693			
GO_REGULATION_OF_WNT_SIGNALING_PATHWAY	282[a]	4.78[a]	0.0000[a]	234[a]	3.88[a]	0.0000[a]	280[a]	4.28[a]	0.0000[a]
GO_REGULATION_OF_WNT_SIGNALING_PATHWAY_PLANAR_CELL_POLARITY_PATHWAY									
GO_WNT_ACTIVATED_RECEPTOR_ACTIVITY	19	0.77	0.7634						
GO_WNT_SIGNALING_PATHWAY	323[a]	4.91[a]	0.0000[a]	267[a]	4.00[a]	0.0000[a]	321[a]	5.24[a]	0.0000[a]
GO_WNT_SIGNALING_PATHWAY_CALCIUM_MODULATING_PATHWAY	38	1.18	0.3029	27	0.78	0.8093	39[a]	1.42[a]	0.1123[a]
GO_WNT_SIGNALOSOME	11	1.15	0.3283				10[a]	1.76[a]	0.0213[a]
HALLMARK_WNT_BETA_CATENIN_SIGNALING	40	0.88	0.6292				40	1.10	0.3301
KEGG_WNT_SIGNALING_PATHWAY	133[a]	2.25[a]	0.0018[a]	106[a]	1.53[a]	0.0872[a]	132[a]	2.13[a]	0.0033[a]
KENNY_CTNNB1_TARGETS_DN	46[a]	3.73[a]	0.0000[a]	45[a]	3.83[a]	0.0000[a]	47[a]	3.53[a]	0.0000[a]
KENNY_CTNNB1_TARGETS_UP	47[a]	2.46[a]	0.0002[a]	42[a]	1.88[a]	0.0156[a]	47[a]	2.30[a]	0.0015[a]
LABBE_WNT3A_TARGETS_DN				53[a]	1.33[a]	0.1791[a]			
LABBE_WNT3A_TARGETS_UP	103[a]	4.53[a]	0.0000[a]	93[a]	3.29[a]	0.0000[a]	102[a]	4.85[a]	0.0000[a]
PID_WNT_CANONICAL_PATHWAY	18[a]	2.53[a]	0.0000[a]	17[a]	1.52[a]	0.0829[a]	19[a]	2.58[a]	0.0004[a]
PID_WNT_NONCANONICAL_PATHWAY	32[a]	2.46[a]	0.0002[a]	28	1.02	0.4977	30[a]	2.31[a]	0.0016[a]
PID_WNT_SIGNALING_PATHWAY	24	1.06	0.4151	17	0.70	0.8845	23	0.91	0.5571
REACTOME_SIGNALING_BY_WNT	61[a]	5.60[a]	0.0000[a]	59[a]	4.80[a]	0.0000[a]	62[a]	5.49[a]	0.0000[a]
WILLERT_WNT_SIGNALING	20[a]	2.05[a]	0.0048[a]	16[a]	2.18[a]	0.0013[a]	20	1.16	0.2784

NOTE. Cell lines: mouse (m) gastric corpus + antrum (ca) ICC-SC lines 2xSCS2F10 (C57BL/6), D2211B, and 2xSCS70 (Immortomouse). D2211B cells were treated with nutlin 3b (30 μmol/L, 72 hours) used as control for nutlin 3a (Table 4). Analysis platforms included mRNA-seq and total RNA-seq (RS) (Illumina HiSeq 2000 and 4000; GSE60854 and GSE139539). RNA-seq data subjected to GSEA[41] Preranked analysis were $\log_2$ normalized expression values (RPKM). Gene set matrix was assembled by searching the Molecular Signatures Database (MSigDB) 6.2[41] for "WNT *AND* FZD" without restrictions. Genes assigned to the indicated gene sets are listed in Supplementary Table 1. [a]These gene sets were significantly enriched in the indicated cell lines and sorted cell populations (FDR $Q < 0.25$). Only positively correlated gene sets are shown for clarity. Gene sets without data were rejected based on the basis of GSEA analysis criteria applied.

Table 3. Stemness-related Gene Sets Enriched in Mouse Gastric ICC-SC by Gene Set Enrichment Analysis

Gene set	2xSCS2F10 (m, ca, RS)			D2211B (m, ca, RS)			2xSCS70 (m, ca, RS)		
	Size	NES	FDR *Q*	Size	NES	FDR *Q*	Size	NES	FDR *Q*
CONRAD_GERMLINE_STEM_CELL									
CONRAD_STEM_CELL							30	0.92	0.5496
KORKOLA_CORRELATED_WITH_POU5F1									
KORKOLA_EMBRYONAL_CARCINOMA_DN									
KORKOLA_EMBRYONAL_CARCINOMA_UP	38[a]	2.23[a]	0.0013[a]	32[a]	1.34[a]	0.1862[a]	36[a]	1.98[a]	0.0147[a]
KORKOLA_SEMINOMA_DN									
KORKOLA_SEMINOMA_UP	37[a]	2.13[a]	0.0037[a]	33[a]	1.44[a]	0.1472[a]	37[a]	1.70[a]	0.0422[a]
KORKOLA_TERATOMA_UP	13[a]	1.75[a]	0.0250[a]	12[a]	1.62[a]	0.0881[a]	12[a]	1.63[a]	0.0501[a]
KORKOLA_YOLK_SAC_TUMOR_UP	20[a]	2.08[a]	0.0040[a]	18	0.88	0.6023	20[a]	1.61[a]	0.0451[a]
LEE_NEURAL_CREST_STEM_CELL_DN				71[a]	1.30[a]	0.1876[a]			
LEE_NEURAL_CREST_STEM_CELL_UP	119[a]	1.69[a]	0.0283[a]	78[a]	1.77[a]	0.0699[a]			
MIKKELSEN_PLURIPOTENT_STATE_DN	8[a]	2.11[a]	0.0031[a]	8[a]	1.75[a]	0.0549[a]	8[a]	1.92[a]	0.0125[a]
MIKKELSEN_PLURIPOTENT_STATE_UP									
MUELLER_PLURINET	27[a] 3	7.26[a]	0.0000[a]	26[a] 5	4.44[a]	0.0000[a]	276[a]	8.21[a]	0.0000[a]

NOTE. Cell lines: mouse (m) gastric corpus + antrum (ca) ICC-SC lines 2xSCS2F10 (C57BL/6), D2211B, and 2xSCS70 (Immortomouse).[21,22] D2211B cells were treated with nutlin 3b (30 μmol/L, 72 hours) used as control for nutlin 3a (Table 4). Analysis platforms included mRNA-seq and total RNA-seq (RS) (Illumina HiSeq 2000 and 4000; GSE60854 and GSE139539). RNA-seq data subjected to GSEA[41] Preranked analysis were $\log_2$ normalized expression values (RPKM). Gene set matrix was assembled by searching the Molecular Signatures Database (MSigDB) 6.2[41] for "Pluripoten*" without restrictions. Genes assigned to the indicated gene sets are listed in Supplementary Table 2. [a]These gene sets were significantly enriched in the indicated cell lines and sorted cell populations (FDR $Q < 0.25$). Only positively correlated gene sets are shown for clarity. Gene sets without data were rejected on the basis of the GSEA analysis criteria applied.

neurotransmission.[11] To establish the organ-level significance of these findings and extend their validity to naturally aged mice, we first measured gastric compliance ex vivo and determined ICC and ICC-SC frequencies and levels of v-kit Hardy-Zuckerman 4 feline sarcoma viral oncogene homolog (KIT) (stem cell factor receptor, a key ICC marker) protein by flow cytometry and Western immunoblotting (WB), respectively. Gastric compliance was reduced in both *klotho* and naturally aged mice (18–24 months old) vs age-matched wild-type (WT) and 4- to 8-week-old controls (Figure 1*A*), indicating impaired ability of the stomach to relax in response to filling. These changes were associated with a decrease in KIT protein and an increase in the DDR-associated histone modification γ-H2A.X (H2A.X phosphorylated at Ser139), a marker of aging[17] (Figure 1*B*). Consistent with a near-linear age-related decline of ICC in adult humans,[15] γ-H2A.X was also up-regulated, whereas KIT, anoctamin 1 (ANO1) (a calcium-activated chloride channel and functionally significant ICC marker), and ETS variant 1 (ETV1) (a transcription factor important for the development of most ICC including all gastric ICC classes[35]) were reduced in gastric corpus muscles of a 49-year-old male patient and a 51-year-old female patient compared with 19-year-old and 23-year-old sex-matched controls (Figure 1*C*). Next, we enumerated ICC and ICC-SC in the hematopoietic marker-negative fraction (to exclude KIT$^+$ mast cells) in the gastric corpus + antrum of a mixture of C57BL/6 and BALB/c mice between 1 and 107 weeks of age using previously established and validated protocols.[20,21,36] Consistent with our previous finding,[37] ICC decreased sharply between 1 and 15 weeks of age and reached minimum at 58 weeks of age (Figure 1*D*). ICC-SC proportions declined more sharply, reaching a plateau before 15 weeks of age, and decreased further to a minimum at 107 weeks. Minima for both ICC and ICC-SC corresponded well to frequencies detected in *klotho* mice.[11] Thus, ICC-SC loss observed in *klotho* mice also occurs during natural aging and likely contributes to ICC depletion and its functional consequences. Our results also indicate that aging-associated changes in ICC can be identified in ~50-year-old humans.

The Canonical Wnt Signaling Pathway Is Enriched in the Interstitial Cell of Cajal Lineage and Overactivated in the Aging Gastric Tunica Muscularis

To determine the molecular mechanisms underlying aging-related ICC-SC/ICC depletion, we first analyzed Wnt signaling-related gene expression in transcriptome profiles obtained by RNA sequencing (RNA-seq) (Illumina mRNA- and total RNA-seq)[22,38] and hybridization (Affymetrix Mouse Genome 430.2 and Affymetrix Human Genome U133 Plus 2.0 microarrays)[22,39,40] using MetaCore Biological Process Network Analysis and Gene Set Enrichment Analysis (GSEA).[41] Published and newly generated data from 3 mouse gastric ICC-SC lines (2xSCS2F10, D2211B, and 2xSCS70 cells) previously

Table 4. Changes in Stemness-, Senescence-, Autophagy-, and DREAM Complex-related Gene Sets in D2211B ICC-SC Treated With the MDM2 Antagonist Nutlin 3a (Control: Nutlin 3b) by Gene Set Enrichment Analysis

		D2211B (m, ca, RS)		
		Nutlin 3a vs 3b		
Matrix	Gene set	Size	NES	FDR *Q*
Stemness	CONRAD_GERMLINE_STEM_CELL	23[b]	-1.37[b]	0.1000[b]
	CONRAD_STEM_CELL			
	KORKOLA_CORRELATED_WITH_POU5F1	16[b]	-1.35[b]	0.0974[b]
	KORKOLA_EMBRYONAL_CARCINOMA_DN			
	KORKOLA_EMBRYONAL_CARCINOMA_UP	32[b]	-1.50[b]	0.0530[b]
	KORKOLA_SEMINOMA_DN			
	KORKOLA_SEMINOMA_UP	33[b]	-1.59[b]	0.0305[b]
	KORKOLA_TERATOMA_UP			
	KORKOLA_YOLK_SAC_TUMOR_UP	18[b]	-1.35[b]	0.0840[b]
	LEE_NEURAL_CREST_STEM_CELL_DN	71	-1.00	0.4883
	LEE_NEURAL_CREST_STEM_CELL_UP	78[b]	-1.74[b]	0.0031[b]
	MIKKELSEN_PLURIPOTENT_STATE_DN			
	MIKKELSEN_PLURIPOTENT_STATE_UP			
	MUELLER_PLURINET	265	-1.49[b]	0.0468[b]
Senescence	BIOCARTA_TEL_PATHWAY	17	-1.18	0.3004
	COURTOIS_SENESCENCE_TRIGGERS			
	DEMAGALHAES_AGING_DN			
	DEMAGALHAES_AGING_UP	36[b]	-1.36[b]	0.2360[b]
	FRIDMAN_SENESCENCE_DN			
	FRIDMAN_SENESCENCE_UP	63[b]	-1.82[b]	0.0042[b]
	GO_CELL_AGING	58	-0.85	0.7943
	GO_MULTICELLULAR_ORGANISM_AGING	21	-0.78	0.8038
	KAMMINGA_SENESCENCE_(DN)	29[a]	-1.27[a]	0.2484[a]
	KEGG_P53_SIGNALING_PATHWAY	60[b]	-1.30[b]	0.2447[b]
	KUMAMOTO_RESPONSE_TO_NUTLIN_3A_DN			
	KUMAMOTO_RESPONSE_TO_NUTLIN_3A_UP			
	ONGUSAHA_TP53_TARGETS	33[a]	2.59[a]	0.0000[a]
	TANG_SENESCENCE_TP53(inhibition)_TARGETS_DN	48[b]	-1.73[b]	0.0088[b]
	TANG_SENESCENCE_TP53(inhibition)_TARGETS_UP	17	-1.19	0.3416
Autophagy	GO_NEGATIVE_REGULATION_OF_AUTOPHAGY	40[b]	-1.50[b]	0.0655[b]
	GO_POSITIVE_REGULATION_OF_AUTOPHAGY	67[b]	-1.42[b]	0.0692[b]
	GO_REGULATION_OF_AUTOPHAGY	211[b]	-1.41[b]	0.0509[b]
	KEGG_REGULATION_OF_AUTOPHAGY	19	1.05	0.3680
	MIZUSHIMA_AUTOPHAGOSOME_FORMATION	18	-0.50	0.9933
DREAM	BIOCARTA_DREAM_PATHWAY	11	-0.74	0.8980
	FISCHER_DREAM_TARGETS	850[b]	-1.47[b]	0.0363[b]
	REICHERT_MITOSIS_LIN9_TARGETS	28[b]	-1.82[b]	0.0010[b]

NOTE. Mouse (m) gastric corpus + antrum (ca) ICC-SC from the line D2211B[21,22] were treated with nutlin 3a or its 150-fold less potent enantiomer nutlin 3b (30 μmol/L, 72 hours) used as control (n = 3/group). Total RNA-seq (RS) was performed on Illumina HiSeq 4000 platform (GSE139539). RNA-seq data subjected to GSEA[41] analysis were normalized expression values (RPKM). Gene set matrices were assembled by searching the Molecular Signatures Database (MSigDB) 6.2[41] for the appropriate terms. Genes assigned to the indicated gene sets are listed in Supplementary Tables 2 and 3. [a,b]These gene sets were significantly enriched (FDR Q <0.25), showing functional [a]up-regulation and [b]down-regulation, respectively, of the pathway in nutlin 3a–treated cells. (For example, genes in the Kamminga_Senescence_(DN) set were down-regulated on serial passage of mouse embryonic fibroblast; thus their relative reduced expression in nutlin 3a–treated D2211B cells indicates up-regulation of senescence-related genes.) Gene sets without data were rejected on the basis of GSEA analysis criteria applied.

established in our laboratory[21,22] and ICC purified from mouse small intestines or colon[38,39] or from human stomachs[40] were studied (footnotes to Tables 1–5). The MetaCore Signal transduction_WNT signaling network (Supplementary Datasets 1) and canonical and noncanonical Wnt pathway-related gene sets from the Molecular Signatures Database (MSigDB) 6.2[41] were significantly represented in the ICC lineage and specifically in all ICC-SC lines, whereas the Wnt calcium-modulating and polar cell planarity pathways were not enriched (Figure 2*A*, Tables 1 and 2, and Supplementary Table 1). GSEA also revealed a significant expression of stemness-related gene sets in the ICC-SC lines (Figure 2B, Table 3, and Supplementary Table 2). Immunohistochemistry indicated the presence of the key Wnt-induced transcription factor catenin beta 1 (CTNNB1) in KIT$^+$ ICC and KIT$^-$ interstitial cells and enteric neurons in young WT mice (Figure 2*C*). These data provide evidence for the presence and activity of the canonical Wnt pathway in the ICC lineage.

Although Wnt signaling is important for the maintenance of stem cells in a self-renewing state,[23,24] excess Wnt signaling is associated with cellular senescence in several tissues of *klotho* mice, which are hypomorphic for α-Klotho,

Table 5. Changes in Apoptosis/Cell Death–related Gene Sets in D2211B ICC-SC Treated With the MDM2 Antagonist Nutlin 3a (Control: Nutlin 3b) by Gene Set Enrichment Analysis

		D2211B (m, ca, RS)		
		Nutlin 3a vs 3b		
Matrix	Gene set	Size	NES	FDR *Q*
Apoptosis/Death	ALCALA_APOPTOSIS	69	-1.15	0.3928
	BIOCARTA_CASPASE_PATHWAY	20[b]	-1.40[b]	0.1714[b]
	BIOCARTA_CHEMICAL_PATHWAY	20[b]	-1.40[b]	0.1789[b]
	BIOCARTA_DEATH_PATHWAY	30	-1.03	0.5466
	BIOCARTA_DNAFRAGMENT_PATHWAY			
	BIOCARTA_FAS_PATHWAY	28	-1.17	0.3569
	BIOCARTA_FREE_PATHWAY			
	BIOCARTA_MITOCHONDRIA_PATHWAY	20[b]	-1.31[b]	0.2215[b]
	BIOCARTA_PTEN_PATHWAY	17[b]	-1.73[b]	0.0438[b]
	DNA_DAMAGE_RESPONSESIGNAL_TRANSDUCTION_RESULTING_IN_INDUCTION_OF_APOPTOSIS			
	DUTTA_APOPTOSIS_VIA_NFKB	24[b]	-1.52[b]	0.1184[b]
	GALI_TP53_TARGETS_APOPTOTIC_DN			
	GALI_TP53_TARGETS_APOPTOTIC_UP			
	GO_ACTIVATION_OF_CYSTEINE_TYPE_ENDOPEPTIDASE_ACTIVITY_INVOLVED_IN_APOPTOTIC_ SIGNALING_PATHWAY			
	GO_AGING	188[b]	-1.34[b]	0.1967[b]
	GO_APOPTOTIC_PROCESS_INVOLVED_IN_DEVELOPMENT			
	GO_APOPTOTIC_PROCESS_INVOLVED_IN_MORPHOGENESIS			
	GO_APOPTOTIC_SIGNALING_PATHWAY	218[b]	-1.33[b]	0.2033[b]
	GO_CELL_AGING	58	-0.85	0.8110
	GO_CELL_DEATH			
	GO_CELL_KILLING	17	-1.23	0.2861
	GO_CYSTEINE_TYPE_ENDOPEPTIDASE_ACTIVITY_INVOLVED_IN_APOPTOTIC_PROCESS			
	GO_CYSTEINE_TYPE_ENDOPEPTIDASE_INHIBITOR_ACTIVITY_INVOLVED_IN_APOPTOTIC_PROCESS			
	GO_CYSTEINE_TYPE_ENDOPEPTIDASE_REGULATOR_ACTIVITY_INVOLVED_IN_APOPTOTIC_PROCESS	26[b]	-1.35[b]	0.1937[b]
	GO_DEATH_RECEPTOR_ACTIVITY			
	GO_DEATH_RECEPTOR_BINDING	15	-0.77	0.8727
	GO_DEVELOPMENTAL_PROGRAMMED_CELL_DEATH			
	GO_EPITHELIAL_CELL_APOPTOTIC_PROCESS	19	-1.10[b]	0.4393
	GO_EXECUTION_PHASE_OF_APOPTOSIS	41[b]	-1.44[b]	0.1574[b]
	GO_EXTRINSIC_APOPTOTIC_SIGNALING_PATHWAY	73	-1.18	0.3542
	GO_EXTRINSIC_APOPTOTIC_SIGNALING_PATHWAY_VIA_DEATH_DOMAIN_RECEPTORS	29	-1.12	0.4160
	GO_HEPATOCYTE_APOPTOTIC_PROCESS			
	GO_INTRINSIC_APOPTOTIC_SIGNALING_PATHWAY	125[b]	-1.30[b]	0.2218[b]
	GO_INTRINSIC_APOPTOTIC_SIGNALING_PATHWAY_BY_P53_CLASS_MEDIATOR	41	-1.04	0.5332
	GO_INTRINSIC_APOPTOTIC_SIGNALING_PATHWAY_IN_RESPONSE_TO_DNA_DAMAGE	58	-1.14	0.3969
	GO_INTRINSIC_APOPTOTIC_SIGNALING_PATHWAY_IN_RESPONSE_TO_DNA_DAMAGE_BY_P53_CLASS_MEDIATOR	25	-0.75	0.8809
	GO_INTRINSIC_APOPTOTIC_SIGNALING_PATHWAY_IN_RESPONSE_TO_ENDOPLASMIC_RETICULUM_STRESS	30	-1.18	0.3474
	GO_LEUKOCYTE_APOPTOTIC_PROCESS	16	-0.51	0.9908
	GO_LYMPHOCYTE_APOPTOTIC_PROCESS	15	-0.53	0.9951
	GO_MULTICELLULAR_ORGANISM_AGING	21	-0.78	0.8750
	GO_NECROPTOTIC_PROCESS	17	-0.96	0.6902
	GO_NECROTIC_CELL_DEATH	24	-0.91	0.7549
	GO_NEGATIVE_REGULATION_OF_APOPTOTIC_SIGNALING_PATHWAY	154[a]	-1.40[a]	0.1850[a]

Table 5. Continued

Matrix	Gene set	D2211B (m, ca, RS) Nutlin 3a vs 3b Size	NES	FDR Q
	GO_NEGATIVE_REGULATION_OF_B_CELL_APOPTOTIC_PROCESS			
	GO_NEGATIVE_REGULATION_OF_CARDIAC_MUSCLE_CELL_APOPTOTIC_PROCESS			
	GO_NEGATIVE_REGULATION_OF_CELL_DEATH			
	GO_NEGATIVE_REGULATION_OF_ENDOPLASMIC_RETICULUM_STRESS_INDUCED_INTRINSIC_APOPTOTIC_SIGNALING_PATHWAY	15[a]	-1.35[a]	0.1928[a]
	GO_NEGATIVE_REGULATION_OF_ENDOTHELIAL_CELL_APOPTOTIC_PROCESS	15	-1.06	0.4993
	GO_NEGATIVE_REGULATION_OF_EPITHELIAL_CELL_APOPTOTIC_PROCESS	20	-1.18	0.3505
	GO_NEGATIVE_REGULATION_OF_EXTRINSIC_APOPTOTIC_SIGNALING_PATHWAY	74[a]	-1.38[a]	0.1771[a]
	GO_NEGATIVE_REGULATION_OF_EXTRINSIC_APOPTOTIC_SIGNALING_PATHWAY_VIA_DEATH_DOMAIN_RECEPTORS	25	-1.13	0.4037
	GO_NEGATIVE_REGULATION_OF_INTRINSIC_APOPTOTIC_SIGNALING_PATHWAY	72[a]	-1.60[a]	0.0945[a]
	GO_NEGATIVE_REGULATION_OF_INTRINSIC_APOPTOTIC_SIGNALING_PATHWAY_BY_P53_CLASS_MEDIATOR	15	-0.87	0.7993
	GO_NEGATIVE_REGULATION_OF_INTRINSIC_APOPTOTIC_SIGNALING_PATHWAY_IN_RESPONSE_TO_DNA_DAMAGE	22[a]	-1.54[a]	0.1181[a]
	GO_NEGATIVE_REGULATION_OF_LEUKOCYTE_APOPTOTIC_PROCESS	28[a]	-1.50[a]	0.1182[a]
	GO_NEGATIVE_REGULATION_OF_LYMPHOCYTE_APOPTOTIC_PROCESS	20[a]	-1.40[a]	0.1641[a]
	GO_NEGATIVE_REGULATION_OF_MUSCLE_CELL_APOPTOTIC_PROCESS	24[a]	-1.74[a]	0.0492[a]
	GO_NEGATIVE_REGULATION_OF_MYELOID_CELL_APOPTOTIC_PROCESS			
	GO_NEGATIVE_REGULATION_OF_NECROTIC_CELL_DEATH			
	GO_NEGATIVE_REGULATION_OF_NEURON_APOPTOTIC_PROCESS	84[a]	-1.38[a]	0.1760[a]
	GO_NEGATIVE_REGULATION_OF_OXIDATIVE_STRESS_INDUCED_INTRINSIC_APOPTOTIC_SIGNALING_PATHWAY	19[a]	-1.32[a]	0.2148[a]
	GO_NEGATIVE_REGULATION_OF_RELEASE_OF_CYTOCHROME_C_FROM_MITOCHONDRIA	16[a]	-1.45[a]	0.1487[a]
	GO_NEGATIVE_REGULATION_OF_STRIATED_MUSCLE_CELL_APOPTOTIC_PROCESS			
	GO_NEGATIVE_REGULATION_OF_T_CELL_APOPTOTIC_PROCESS			
	GO_NEURON_APOPTOTIC_PROCESS	28	-1.17	0.3608
	GO_NEURON_DEATH	34	-1.21	0.3143
	GO_PEPTIDASE_ACTIVATOR_ACTIVITY_INVOLVED_IN_APOPTOTIC_PROCESS	15	-0.88	0.7897
	GO_POSITIVE_REGULATION_OF_APOPTOTIC_SIGNALING_PATHWAY	132[b]	-1.30[b]	0.2155[b]
	GO_POSITIVE_REGULATION_OF_CELL_DEATH	444[b]	-1.40[b]	0.1889[b]
	GO_POSITIVE_REGULATION_OF_CYSTEINE_TYPE_ENDOPEPTIDASE_ACTIVITY_INVOLVED_IN_APOPTOTIC_SIGNALING_PATHWAY			
	GO_POSITIVE_REGULATION_OF_ENDOTHELIAL_CELL_APOPTOTIC_PROCESS			
	GO_POSITIVE_REGULATION_OF_EPITHELIAL_CELL_APOPTOTIC_PROCESS	16[b]	-1.59[b]	0.0851[b]
	GO_POSITIVE_REGULATION_OF_EXTRINSIC_APOPTOTIC_SIGNALING_PATHWAY	40	-0.90	0.7637
	GO_POSITIVE_REGULATION_OF_EXTRINSIC_APOPTOTIC_SIGNALING_PATHWAY_IN_ABSENCE_OF_LIGAND			
	GO_POSITIVE_REGULATION_OF_EXTRINSIC_APOPTOTIC_SIGNALING_PATHWAY_VIA_DEATH_DOMAIN_RECEPTORS			
	GO_POSITIVE_REGULATION_OF_INTRINSIC_APOPTOTIC_SIGNALING_PATHWAY	42[b]	-1.27[b]	0.2429[b]
	GO_POSITIVE_REGULATION_OF_LEUKOCYTE_APOPTOTIC_PROCESS	18	-1.00	0.5998
	GO_POSITIVE_REGULATION_OF_LYMPHOCYTE_APOPTOTIC_PROCESS			
	GO_POSITIVE_REGULATION_OF_MITOCHONDRIAL_OUTER_MEMBRANE_PERMEABILIZATION_INVOLVED_IN_APOPTOTIC_SIGNALING_PATHWAY	29	-1.26	0.2592
	GO_POSITIVE_REGULATION_OF_MUSCLE_CELL_APOPTOTIC_PROCESS			
	GO_POSITIVE_REGULATION_OF_NEURON_APOPTOTIC_PROCESS	38	-0.65	0.9504
	GO_POSITIVE_REGULATION_OF_RELEASE_OF_CYTOCHROME_C_FROM_MITOCHONDRIA	22	-0.73	0.8967
	GO_POSITIVE_REGULATION_OF_T_CELL_APOPTOTIC_PROCESS			
	GO_REGULATION_OF_APOPTOTIC_SIGNALING_PATHWAY	278[b]	-1.34[b]	0.1941[b]
	GO_REGULATION_OF_B_CELL_APOPTOTIC_PROCESS	15	-0.95	0.6934

Table 5. Continued

Matrix	Gene set	D2211B (m, ca, RS) Nutlin 3a vs 3b Size	NES	FDR *Q*
	GO_REGULATION_OF_CELL_DEATH	18[b]	-1.35[b]	0.1921[b]
	GO_REGULATION_OF_CYSTEINE_TYPE_ENDOPEPTIDASE_ACTIVITY_INVOLVED_IN_APOPTOTIC_SIGNALING_PATHWAY			
	GO_REGULATION_OF_ENDOPLASMIC_RETICULUM_STRESS_INDUCED_INTRINSIC_APOPTOTIC_SIGNALING_PATHWAY	26	-1.13	0.4100
	GO_REGULATION_OF_ENDOTHELIAL_CELL_APOPTOTIC_PROCESS	24[b]	-1.39[b]	0.1691[b]
	GO_REGULATION_OF_EPITHELIAL_CELL_APOPTOTIC_PROCESS	36[b]	-1.61[b]	0.0965[b]
	GO_REGULATION_OF_EXTRINSIC_APOPTOTIC_SIGNALING_PATHWAY	115	-1.26	0.2589
	GO_REGULATION_OF_EXTRINSIC_APOPTOTIC_SIGNALING_PATHWAY_IN_ABSENCE_OF_LIGAND	34[b]	-1.47[b]	0.1340[b]
	GO_REGULATION_OF_EXTRINSIC_APOPTOTIC_SIGNALING_PATHWAY_VIA_DEATH_DOMAIN_RECEPTORS	41	-1.09	0.4553
	GO_REGULATION_OF_FIBROBLAST_APOPTOTIC_PROCESS			
	GO_REGULATION_OF_INTRINSIC_APOPTOTIC_SIGNALING_PATHWAY	115[b]	-1.50[b]	0.1199[b]
	GO_REGULATION_OF_INTRINSIC_APOPTOTIC_SIGNALING_PATHWAY_BY_P53_CLASS_MEDIATOR	18	-0.87	0.7938
	GO_REGULATION_OF_INTRINSIC_APOPTOTIC_SIGNALING_PATHWAY_IN_RESPONSE_TO_DNA_DAMAGE	29[b]	-1.53[b]	0.1159[b]
	GO_REGULATION_OF_INTRINSIC_APOPTOTIC_SIGNALING_PATHWAY_IN_RESPONSE_TO_DNA_DAMAGE_BY_ P53_CLASS_MEDIATOR			
	GO_REGULATION_OF_LEUKOCYTE_APOPTOTIC_PROCESS	51[b]	-1.43[b]	0.1687[b]
	GO_REGULATION_OF_LYMPHOCYTE_APOPTOTIC_PROCESS	37	-1.24	0.2789
	GO_REGULATION_OF_MESENCHYMAL_CELL_APOPTOTIC_PROCESS			
	GO_REGULATION_OF_MITOCHONDRIAL_MEMBRANE_PERMEABILITY_INVOLVED_IN_APOPTOTIC_PROCESS	19	-0.94	0.7132
	GO_REGULATION_OF_MITOCHONDRIAL_OUTER_MEMBRANE_PERMEABILIZATION_INVOLVED_IN_ APOPTOTIC_SIGNALING_PATHWAY	33	-1.12	0.4142
	GO_REGULATION_OF_MUSCLE_CELL_APOPTOTIC_PROCESS	32[b]	-1.69[b]	0.0529[b]
	GO_REGULATION_OF_MYELOID_CELL_APOPTOTIC_PROCESS	15[b]	-1.52[b]	0.1223[b]
	GO_REGULATION_OF_NECROPTOTIC_PROCESS			
	GO_REGULATION_OF_NECROTIC_CELL_DEATH	21	-1.16	0.3621
	GO_REGULATION_OF_NEURON_APOPTOTIC_PROCESS	127[b]	-1.37[b]	0.1748[b]
	GO_REGULATION_OF_OXIDATIVE_STRESS_INDUCED_INTRINSIC_APOPTOTIC_SIGNALING_PATHWAY	25	-1.19	0.3481
	GO_REGULATION_OF_PROTEIN_INSERTION_INTO_MITOCHONDRIAL_MEMBRANE_INVOLVED_ IN_APOPTOTIC_SIGNALING_PATHWAY	23	-1.24	0.2794
	GO_REGULATION_OF_RELEASE_OF_CYTOCHROME_C_FROM_MITOCHONDRIA	37	-1.10	0.4359
	GO_REGULATION_OF_SMOOTH_MUSCLE_CELL_APOPTOTIC_PROCESS			
	GO_REGULATION_OF_STRIATED_MUSCLE_CELL_APOPTOTIC_PROCESS	17[b]	-1.55[b]	0.1150[b]
	GO_REGULATION_OF_T_CELL_APOPTOTIC_PROCESS	21[b]	-1.61[b]	0.0859[b]
	GO_REGULATION_OF_THYMOCYTE_APOPTOTIC_PROCESS			
	GO_RELEASE_OF_CYTOCHROME_C_FROM_MITOCHONDRIA	17[b]	-1.30[b]	0.2178[b]
	GO_T_CELL_APOPTOTIC_PROCESS			
	GRAESSMANN_APOPTOSIS_BY_DOXORUBICIN_DN			
	GRAESSMANN_APOPTOSIS_BY_DOXORUBICIN_UP			
	GRAESSMANN_APOPTOSIS_BY_SERUM_DEPRIVATION_DN	174[b]	-1.41[b]	0.1837[b]
	GRAESSMANN_APOPTOSIS_BY_SERUM_DEPRIVATION_UP	403[b]	-1.51[b]	0.1214[b]
	GRAESSMANN_RESPONSE_TO_MC_AND_DOXORUBICIN_DN			
	GRAESSMANN_RESPONSE_TO_MC_AND_DOXORUBICIN_UP			
	GRAESSMANN_RESPONSE_TO_MC_AND_SERUM_DEPRIVATION_DN	60[b]	-1.36[b]	0.1810[b]
	GRAESSMANN_RESPONSE_TO_MC_AND_SERUM_DEPRIVATION_UP	155[b]	-1.92[b]	0.0090[b]
	HALLMARK_APOPTOSIS	133[b]	-1.37[b]	0.1768[b]
	HAMAI_APOPTOSIS_VIA_TRAIL_DN	107[b]	-1.48[b]	0.1388[b]

Table 5. Continued

Matrix	Gene set	D2211B (m, ca, RS) Nutlin 3a vs 3b Size	NES	FDR *Q*
	HAMAI_APOPTOSIS_VIA_TRAIL_UP	473	-0.80	0.8525
	HERNANDEZ_MITOTIC_ARREST_BY_DOCETAXEL_1_DN	29[b]	-1.90[b]	0.0045[b]
	HERNANDEZ_MITOTIC_ARREST_BY_DOCETAXEL_1_UP	21[b]	-1.54[b]	0.1268[b]
	HERNANDEZ_MITOTIC_ARREST_BY_DOCETAXEL_2_DN			
	HERNANDEZ_MITOTIC_ARREST_BY_DOCETAXEL_2_UP	45	-0.93	0.7156
	INDUCTION_OF_APOPTOSIS_BY_EXTRACELLULAR_SIGNALS	21[b]	-1.30[b]	0.2258[b]
	INDUCTION_OF_APOPTOSIS_BY_INTRACELLULAR_SIGNALS	16	-1.13	0.4119
	KEGG_APOPTOSIS	66	-1.23	0.2886
	MARTORIATI_MDM4_TARGETS_NEUROEPITHELIUM_DN	66[b]	-1.40[b]	0.1670[b]
	MARTORIATI_MDM4_TARGETS_NEUROEPITHELIUM_UP	135	-0.76	0.8760
	NEURON_APOPTOSIS			
	PID_CASPASE_PATHWAY	45[b]	-1.59[b]	0.0931[b]
	RAMJAUN_APOPTOSIS_BY_TGFB1_VIA_MAPK1_DN			
	RAMJAUN_APOPTOSIS_BY_TGFB1_VIA_MAPK1_UP			
	RAMJAUN_APOPTOSIS_BY_TGFB1_VIA_SMAD4_DN			
	RAMJAUN_APOPTOSIS_BY_TGFB1_VIA_SMAD4_UP			
	REACTOME_APOPTOSIS	123	-1.11	0.4361
	REACTOME_APOPTOSIS_INDUCED_DNA_FRAGMENTATION			
	REACTOME_APOPTOTIC_CLEAVAGE_OF_CELL_ADHESION_PROTEINS			
	REACTOME_APOPTOTIC_CLEAVAGE_OF_CELLULAR_PROTEINS	27[b]	-1.40[b]	0.1744[b]
	REACTOME_APOPTOTIC_EXECUTION_PHASE	41[b]	-1.46[b]	0.1410[b]
	REACTOME_CELL_DEATH_SIGNALLING_VIA_NRAGE_NRIF_AND_NADE	50[b]	-1.29[b]	0.2247[b]
	REACTOME_EXTRINSIC_PATHWAY_FOR_APOPTOSIS			
	REACTOME_INTRINSIC_PATHWAY_FOR_APOPTOSIS	27[b]	-1.29[b]	0.2240[b]
	REACTOME_NRAGE_SIGNALS_DEATH_THROUGH_JNK	35	-1.24[b]	0.2787
	REACTOME_NRIF_SIGNALS_CELL_DEATH_FROM_THE_NUCLEUS			
	REACTOME_REGULATION_OF_APOPTOSIS	53	-0.82	0.8324
	REACTOME_ROLE_OF_DCC_IN_REGULATING_APOPTOSIS			
	REGULATION_OF_NEURON_APOPTOSIS			
	SA_CASPASE_CASCADE	15	-0.85	0.8067
	SA_FAS_SIGNALING			
	YAN_ESCAPE_FROM_ANOIKIS	17[a]	-1.64[a]	0.0849[a]
	ZEILSTRA_CD44_TARGETS_DN			
	ZEILSTRA_CD44_TARGETS_UP			

NOTE. Mouse (m) gastric corpus + antrum (ca) ICC-SC from the line D2211B[21,22] were treated with nutlin 3a or its 150-fold less potent enantiomer nutlin 3b (30 μmol/L, 72 hours) used as control (n = 3/group). Total RNA-seq (RS) was performed on Illumina HiSeq 4000 platform (GSE139539). RNA-seq data subjected to GSEA[41] analysis were normalized expression values (RPKM). Gene set matrix was assembled by searching the Molecular Signatures Database (MSigDB) 6.2[41] for "Apoptosis OR Apoptotic OR Death" (in the title or description). Genes assigned to the indicated gene sets are listed in Supplementary Table 4. [a,b]These gene sets were significantly enriched (FDR *Q* $<$0.25), showing functional [a]up-regulation and [b]down-regulation, respectively, of the pathway in nutlin 3a–treated cells. (For example, genes in the Yan_Escape_from_Anoikis set were down-regulated; thus their relative reduced expression in nutlin 3a–treated D2211B cells indicates functional up-regulation of anoikis-related genes). Gene sets without data were rejected on the basis of the GSEA analysis criteria applied.

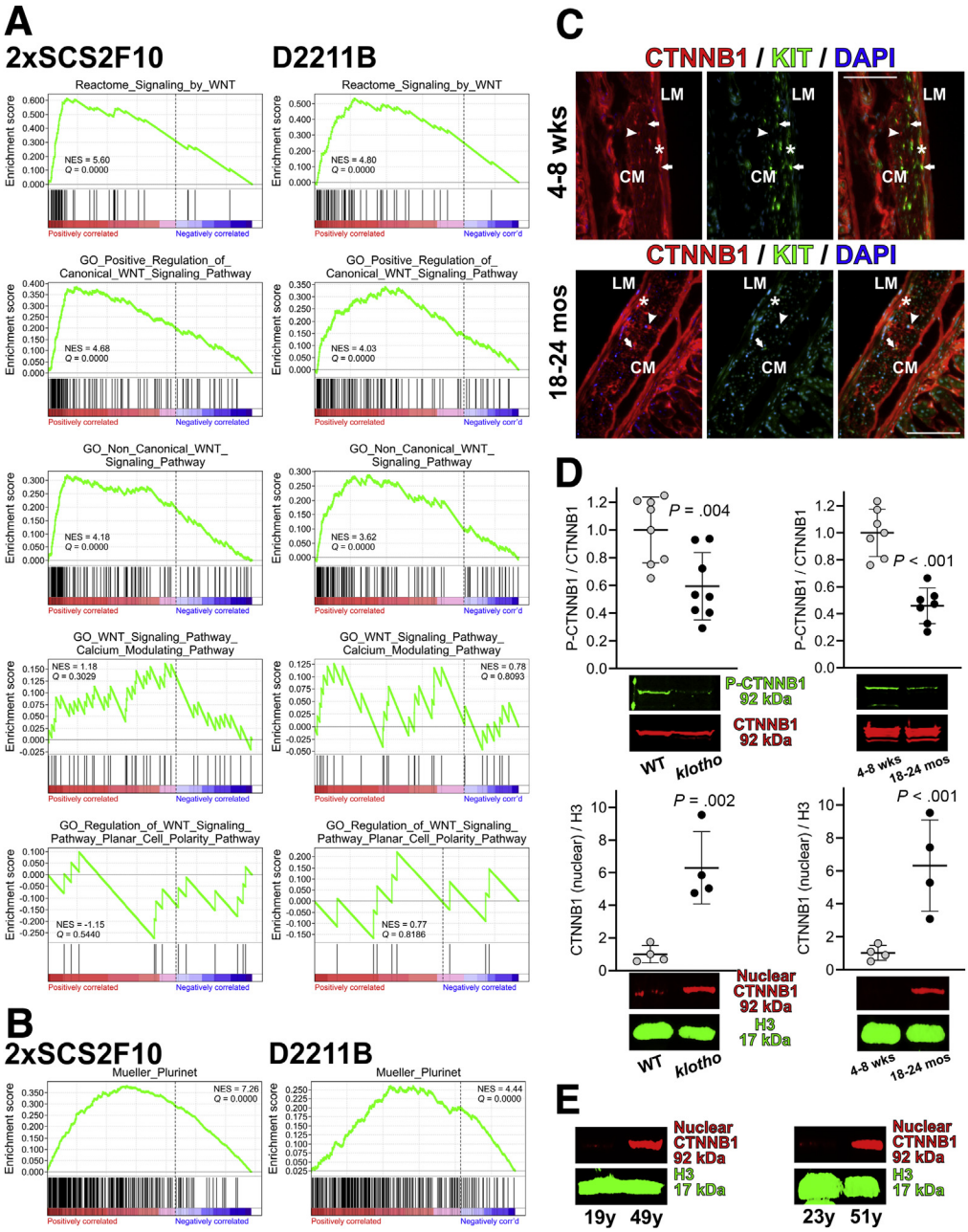

Figure 2. The canonical Wnt signaling pathway is enriched in the ICC lineage and overactivated in the aging gastric tunica muscularis. (*A*) Enrichment of canonical and noncanonical Wnt pathways but not the calcium-modulating or planar cell polarity pathways in 2xSCS2F10 and D2211B ICC-SC lines analyzed by mRNA-seq and GSEA. *Vertical lines* indicate genes ranked by RPKM values. Gene sets with FDR *Q* value <0.25 and positive NES were considered significantly enriched. See further data and gene sets analyzed in Table 2 and Supplementary Table 1. (*B*) Enrichment of stemness-related genes in 2xSCS2F10 and D2211B ICC-SC lines by GSEA. See further data and gene sets analyzed in Table 3 and Supplementary Table 2. (*C*) Immunoreactivity for CTNNB1 (*red*), KIT (*green*), and DAPI (*blue*) in 5-μm cryosections of gastric tunica muscularis tissues from young and old mice (n = 3/group). *Scale bars*, 25 μm. CTNNB1 was expressed in ICC (*arrows*), KIT$^-$ interstitial cells (*arrowheads*), and enteric neurons (*asterisks*) in both young and old mice. Note reduced KIT$^+$ ICC in the old mouse. (*D*) CTNNB1 phosphorylation on Ser33/Ser37/Thr41 (P-CTNNB1) was reduced and nuclear CTNNB1 was increased in gastric corpus + antrum tissues of *klotho* mice vs WT controls and in old mice vs young controls (n = 4–8/group), indicating age-related overactivation of Wnt signaling. *P* values are from Mann-Whitney rank sum tests. (*E*) Up-regulated nuclear CTNNB1 protein in gastric corpus muscles of 49-year-old and 51-year-old patients vs 19-year-old and 23-year-old controls. CM, circular muscle; LM, longitudinal muscle.

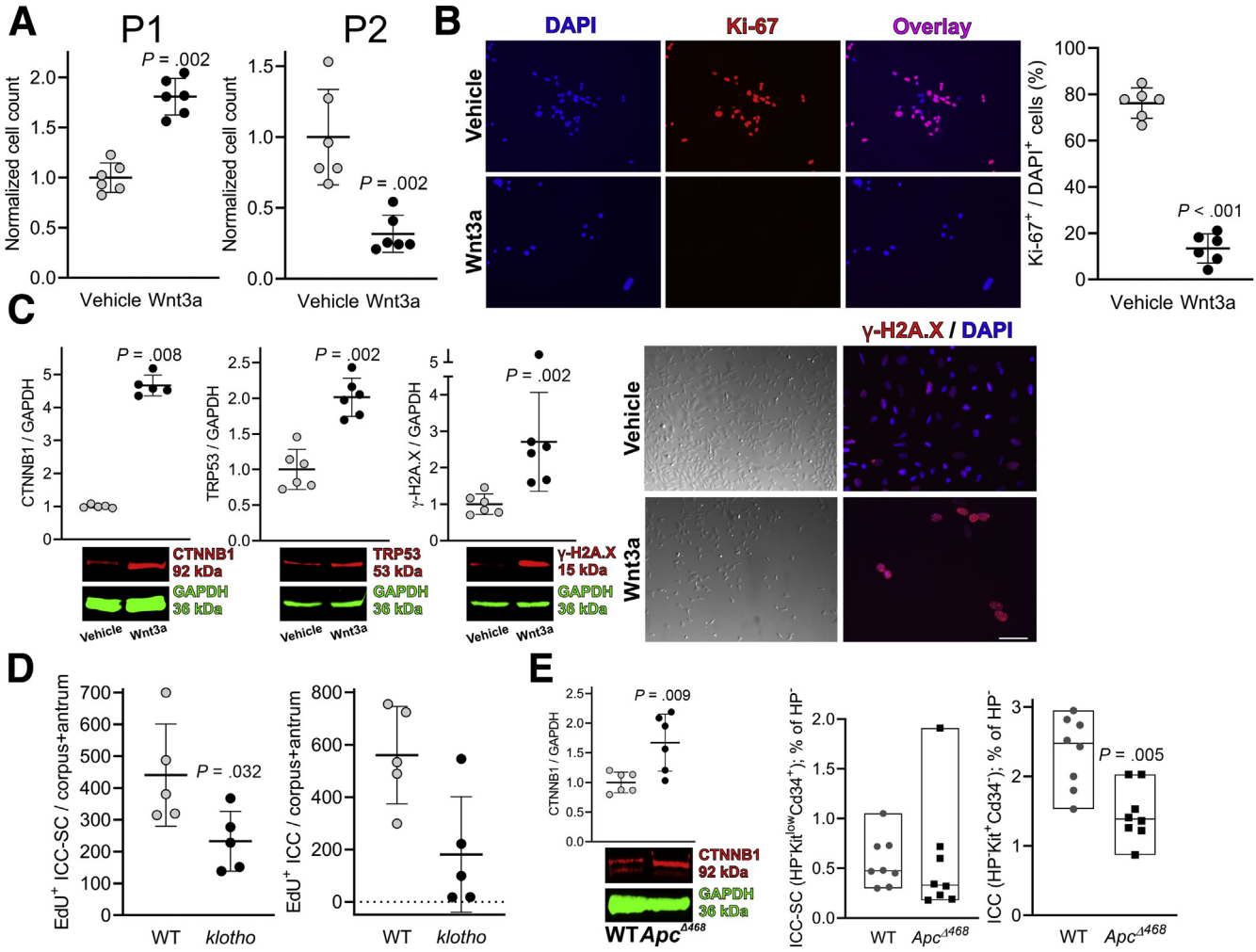

Figure 3. Prolonged overactivation of canonical Wnt signaling causes paradoxical inhibition of ICC-SC proliferation. (*A*) 50,000 D2211B ICC-SC were cultured in the presence or absence of 30 ng/mL mouse recombinant Wnt3a (n = 12/group). Cell counts were determined when Wnt3a-treated cells reached confluence at 8 days of culturing (P1). Then 50,000 cells were re-plated (12 cultures/group) and counted when the controls reached confluence at 15 days (P2). ICC-SC counts in the Wnt3a-treated cultures were reduced after an initial increase. *P* values are from Mann-Whitney rank sum tests. (*B*) Reduced proliferation of D2211B ICC-SC detected by Ki-67 immunofluorescence after 15-day stimulation with Wnt3a (30 ng/mL). Nuclei were counterstained with DAPI. *P* value is from Mann-Whitney rank sum test. (*C*) Fifteen-day exposure of D2211B cells to 30 ng/mL Wnt3a up-regulated CTNNB1 and the DDR-associated proteins TRP53 and γ-H2A.X by WB and γ-H2A.X by immunofluorescence (n = 6/group). *P* values are from Mann-Whitney rank sum tests. (*D*) Reduced EdU^+ proliferating ICC-SC and ICC detected in the gastric tunica muscularis of *klotho* vs WT mice by flow cytometry (n = 5/group). *P* values are from Mann-Whitney rank sum tests. (*E*) Up-regulated CTNNB1 and reduced ICC-SC and ICC in gastric tunica muscularis of $APC^{\Delta 468}$ vs WT mice (n = 6–8/group). *P* values are from Mann-Whitney rank sum tests.

a Wnt inhibitor.[28] To examine whether Wnt signaling increases in mouse and human gastric tunica muscularis with age, we analyzed levels of unstable and nuclear CTNNB1 proteins in the gastric tunica muscularis of *klotho* and naturally aged mice as well as in human gastric muscles. CTNNB1 phosphorylation on Ser33/Ser37/Thr41, which targets CTNNB1 for proteasomal degradation, rendering it unstable, was reduced in both *klotho* and naturally aged mice (Figure 2*D*), suggesting an activated state. Indeed, nuclear CTNNB1, a hallmark of active Wnt signaling, was increased in both *klotho* and aged mice (Figure 2*D*). We also detected similar increases in nuclear CTNNB1 in a 49-year-old patient vs a 19-year-old patient and a 51-year-old patient vs a 23-year-old patient (Figure 2*E*). Taken together, these findings indicate that Wnt/CTNNB1 signaling is activated in gastric tissues with increasing age.

Prolonged Overactivation of Canonical Wnt Signaling Causes Paradoxical Inhibition of Interstitial Cell of Cajal Stem Cell Proliferation

Overactive Wnt signaling from reduced Klotho levels can lead to cancer[42] or induce cellular senescence (growth arrest).[28] To establish a mechanistic link between the observed age-related activation of Wnt/CTNNB1 signaling

in gastric muscles and ICC-SC depletion, we cultured D2211B ICC-SC with 30 ng/mL mouse recombinant Wnt3a as an inducer of canonical Wnt signaling. Indeed, we found increased ICC-SC growth after 8 days of treatment but suppressed growth after 15 days by counting cell numbers and by immunostaining for Ki-67, a cell proliferation marker (Figure 3*A* and *B*). WB and immunofluorescence analysis showed that the up-regulation of CTNNB1 in response to 15-day exposure of ICC-SC to Wnt3a was also associated with increased levels of the DDR marker γ-H2A.X and the DDR response mediator protein TRP53 (Figure 3*C*). These findings indicate that prolonged exposure of ICC-SC to high concentration of a canonical Wnt ligand can induce some form of ICC-SC growth arrest after stimulation of proliferation.

To demonstrate reduced ICC-SC proliferation in the context of aging in vivo, we analyzed, after daily exposure for 2 weeks, the incorporation of the modified deoxyribonucleoside and DNA synthesis marker 5-ethynyl-2′-deoxyuridine (EdU) into ICC-SC and ICC of the gastric corpus + antrum of *klotho* and WT mice by flow cytometry. Indeed, the numbers of EdU^+ ICC-SC that have undergone DNA replication at least once during the 2-week period of injections were reduced in *klotho* mice compared with WT mice (Figure 3*D*), indicating reduced ICC-SC proliferation with age. EdU^+ ICC were less consistently reduced, suggesting that this population may have mainly contained cells that had been labeled as ICC-SC during the early days of the EdU treatment protocol before differentiating into ICC. Indeed, although the total numbers of EdU^+ gastric ICC-SC and ICC were very similar, they represented 27% ± 12% (mean ± standard deviation) of all ICC-SC but only 3% ± 1% of all ICC ($P = .008$, Mann-Whitney rank sum test).

Next, to demonstrate a causal role for chronically elevated canonical Wnt signaling in age-related ICC loss in vivo, we enumerated ICC-SC and ICC in the gastric corpus + antrum $APC^{\Delta 468}$ mice, which lack functional adenomatous polyposis coli (APC) protein, an essential component of the CTNNB1 destruction complex and an endogenous inhibitor of the Wnt-CTNNB1 pathway.[34] The proportions of ICC-SC and particularly differentiated ICC were reduced in the stomach of $APC^{\Delta 468}$ mice with chronically elevated CTNNB1 levels (Figure 3*E*). These findings provide in vivo mechanistic evidence for canonical Wnt signaling causing aging-associated ICC-SC growth arrest leading to ICC decline.

Transformation Related Protein 53 Is Up-regulated in the Aging Gastric Tunica Muscularis and Inhibits Interstitial Cell of Cajal Stem Cell Growth

To establish a causal relationship between excess CTNNB1 and TRP53 up-regulation,[29] we first verified that overexpression of constitutively active *Ctnnb1* increased TRP53 protein levels in 2xSCS2F10 ICC-SC (Figure 4*A*). Conversely, small interfering RNA (siRNA)-mediated *Ctnnb1* knockdown down-regulated TRP53 protein levels in D2211B cells (Figure 4*A*). These results strongly support a role for CTNNB1 in regulating TRP53 in ICC-SC. By WB and immunohistochemistry, we found increased TRP53 protein levels in gastric tunica muscularis of both *klotho* and naturally aged mice and in the 49-year-old and 51-year-old patients vs their controls (Figure 4*B* and *C*). mRNA for sestrin 2 (*Sesn2*), sestrin 3 (*Sesn3*), and cyclin-dependent kinase 1a (*Cdkn1a*; also known as $p21^{Waf1/Cip1}$), which are established transcriptional targets of TRP53,[43] were robustly increased in *klotho* mice and moderately in aged mice by real-time quantitative reverse transcription polymerase chain reaction (RT-qPCR) (Figure 4*D*). To investigate whether elevated TRP53 signaling could recapitulate Wnt/CTNNB1-induced ICC-SC loss, we exposed D2211B cells to 10–30 μmol/L nutlin 3a, an inhibitor of the mouse double minute 2 E3 ubiquitin-protein ligase (a negative regulator of TRP53), which belongs to a drug class currently in early clinical trials.[44,45] Forty-eight-hour nutlin 3a treatment of ICC-SC up-regulated TRP53 protein, *Sesn2*, *Sesn3,* and *Cdkn1a* mRNA, and γ-H2A.X protein levels (Figure 4*E*) and dose-dependently reduced ICC-SC growth (Figure 4*F*). These results indicate that TRP53 likely plays an important role in Wnt-induced, aging-associated ICC-SC and ICC depletion.

Transformation Related Protein 53 Activation Inhibits Interstitial Cell of Cajal Stem Cell Growth by Reducing Cell Proliferation and Clonogenicity via Down-regulation of Self-renewal Genes and Cell Cycle Arrest

To investigate the spectrum of TRP53 effects that may underlie the observed inhibition of ICC-SC growth, we performed total RNA-seq in D2211B cells maintained under conditions nonpermissive for the expression of the tsA58-mutant SV40 large T antigen (tsTAg), which was undetectable by immunofluorescence and WB,[21] enabling senescence pathways.[46] D2211B cultures were treated with 30 μmol/L nutlin 3a or nutlin 3b for 72 hours (n = 3/group). Differential enrichment of MSigDB 6.2 gene sets assembled into matrices related to TRP53 functions—senescence, autophagy, cell cycle arrest by the DREAM (dimerization partner, RB-like, E2F and multi-vulval class B) complex, and apoptosis/cell death[30–33]—was analyzed by GSEA (Tables 4 and 5, Supplementary Tables 3 and 4). GSEA verified the up-regulated expression of canonical TRP53 target genes in nutlin 3a–treated cells vs nutlin 3b–treated controls (Figure 5*A*). Autophagy-related gene sets were mainly down-regulated (3/5). Unexpectedly, most gene sets covering apoptosis/cell death (43/106), cellular senescence (4/10), and quiescence (DREAM complex targets; 2/3), which are typically up-regulated with age, were also down-regulated in nutlin 3a–treated ICC-SC. Up-regulated gene sets were restricted to 12/106 apoptosis/cell death-related and 2/10 senescence-related sets (including the set containing canonical TRP53 target genes). Consistent with GSEA analysis, WB indicated significantly reduced cleaved caspase 3 (CL.CASP3), a marker of apoptosis, and light chain 3B isoform II, a marker for autophagy, in nutlin 3a–treated D2211B cells (Figure 5*B*). Histochemical analysis of

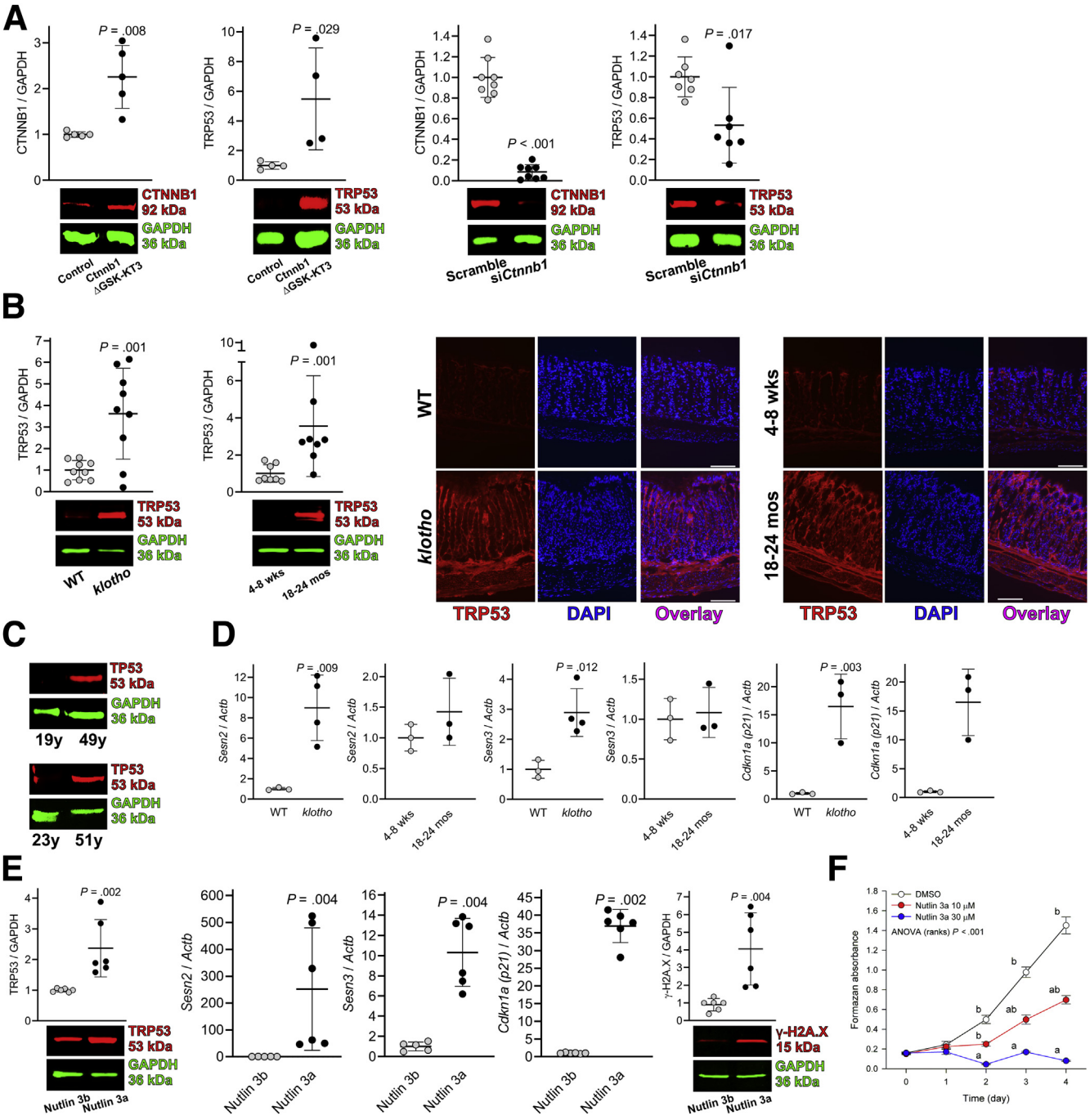

Figure 4. TRP53 is up-regulated in the aging gastric tunica muscularis and inhibits ICC-SC growth. (*A*) Overexpression of constitutively active *Ctnnb1* in 2XSCS2F10 ICC-SC by nucleofection increased TRP53 protein levels (n = 5/group). The siRNA-mediated knockdown of *Ctnnb1* down-regulated TRP53 protein expression in D2211B cells (n = 8/group). Efficacy of RNA interference against *Ctnnb1* was verified by WB (n = 8/group). *P* values are from Mann-Whitney rank sum tests. (*B*) *Left panels:* increased TRP53 protein in *klotho* mouse gastric lysates compared with WT controls and in old vs young mice (n = 8–9/group). *Right panels:* immunoreactivity for TRP53 (*red*) and nuclear DAPI (*blue*) in cryosections of gastric tissues from *klotho* and WT control (n = 3/group) and young and old mice (n = 3/group). Note increased TRP53 protein in both the tunica mucosa and the tunica muscularis. *P* values are from Mann-Whitney rank sum tests. (*C*) Up-regulated TRP53 protein in the gastric corpus tunica muscularis of 49-year-old and 51-year-old patients vs 19-year-old and 23-year-old patients. (*D*) Increased expression of TRP53 transcriptional target genes *Sesn2*, *Sesn3,* and *Cdkn1a* (n = 3–4/group) by RT-qPCR in gastric tissues of *klotho* mice compared with WT controls. More modest changes were seen in old mice compared with young controls (n = 3–4/group). *P* values are from *t* tests. (*E*) Treatment with nutlin 3a, inhibitor of the TRP53-degrading E3 ubiquitin ligase MDM2 (30 μmol/L), of D2211B cells increased TRP53 and γ-H2A.X protein levels by WB (72 hours; n = 4/group) and the expression of TRP53 target genes *Sesn2*, *Sesn3,* and *Cdkn1a* by RT-qPCR (48 hours) vs treatment with the 150-fold less potent enantiomer nutlin 3b (n = 5–6/group). *P* values are from Mann-Whitney rank sum tests. (*F*) Nutlin 3a dose-dependently reduced D2211B proliferation by MTS assay (n = 7–8/group). *P* values are from Kruskal-Wallis one-way ANOVA (ANOVA on ranks). Groups not sharing the same superscript are different by multiple comparisons ($P < .05$; Tukey tests).

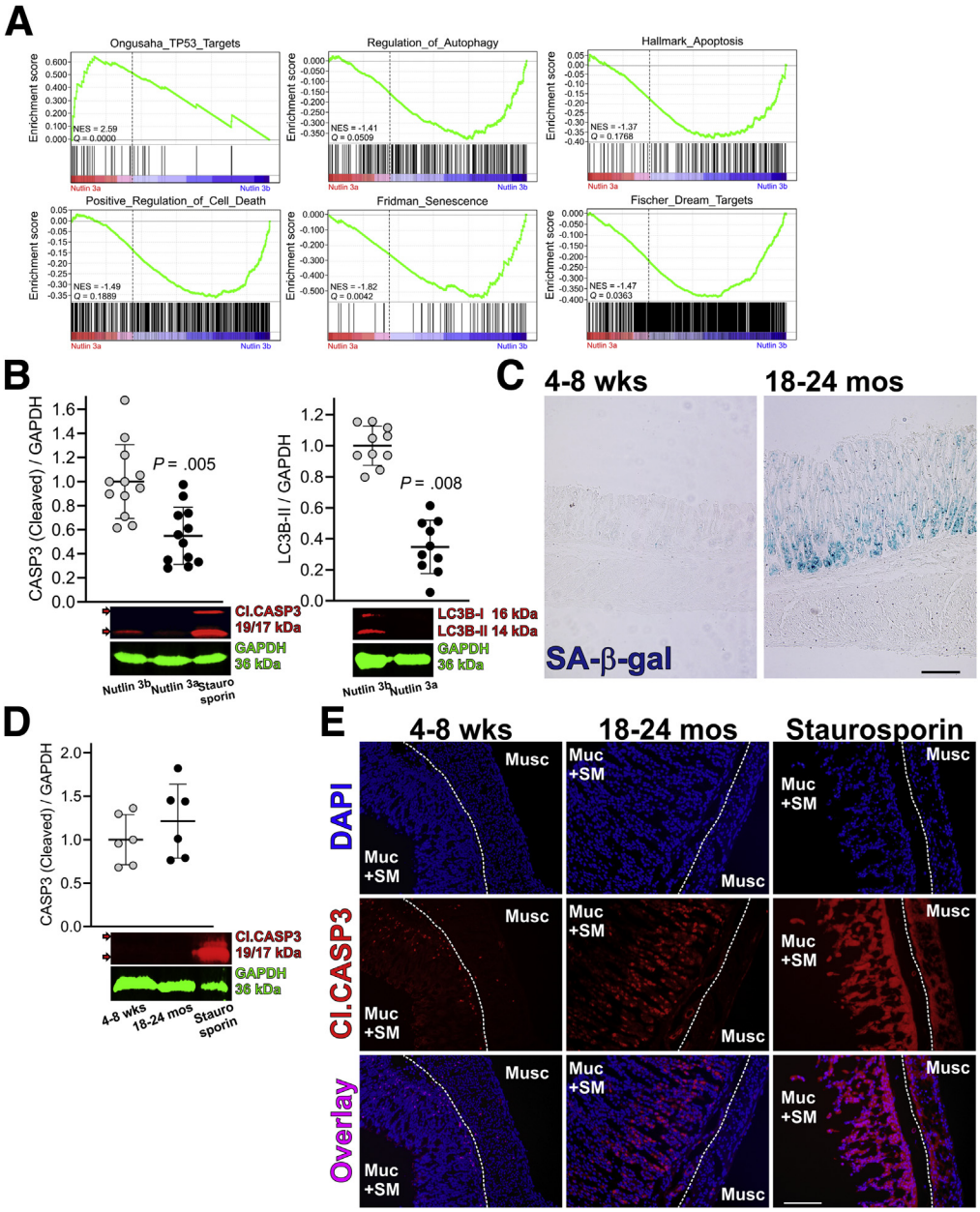

Figure 5. Cell death–, apoptosis-, autophagy-, senescence-, and quiescence-related pathways are not stimulated by TRP53 up-regulation in ICC-SC. (*A*) GSEA of total RNA-seq data showing enrichment of TRP53 target genes and depletion of cell death–, apoptosis-, autophagy-, senescence-, and quiescence (DREAM complex)-related genes in D2211B ICC-SC treated with nutlin 3a vs cells treated with nutlin 3b (30 μmol/L, 72 hours; n = 3/group). *Vertical lines* indicate genes. Negative NES and FDA Q <0.25 indicate significant depletion. See all data and gene sets analyzed in Tables 4 and 5 and in Supplementary Tables 3 and 4. (*B*) Nutlin 3a (30 μmol/L, 72 hours) in D2211B cells reduced CL.CASP3 (n = 12/group) and light chain 3B isoform II (LC3B-II) levels vs nutlin 3b (n = 7/group). Staurosporin (3 μmol/L, 24 hours) was used as a positive control for apoptosis induction. *P* values are from Mann-Whitney rank sum tests. (*C*) Senescent cells detected by SA-β-Gal activity were increased in the gastric mucosa of old (18–24 months) vs young mice (4–8 weeks). No SA-β-gal activity was evident in the gastric muscle layers of either old or young mice. (*D* and *E*) Apoptosis detected in the gastric corpus + antrum tunica muscularis by CL.CASP3 immunoblotting (*D*) and in the gastric corpus + antrum (full thickness) by immunohistochemistry (*E*) in old (18–24 months) vs young mice (4–8 weeks). CL.CASP3 activity was low in the gastric muscle layers of both old and young mice and did not increase with age. Positive controls were exposed to staurosporin (3 μmol/L, 24 hours; n = 6/group). Data in *D* were analyzed by Mann-Whitney rank sum test.

senescence-associated β-galactosidase (SA-β-gal) activity[47] in aged and young mouse stomachs only revealed increased cellular senescence in the gastric mucosa but not in the tunica muscularis of 18- to 24-month-old mice (Figure 5*C*). A similar, mucosa-restricted increase in SA-β-gal activity compared with WT mice was previously reported in *klotho* small intestines.[28] In aged mice, CL.CASP3 only showed a small increase relative to young animals by

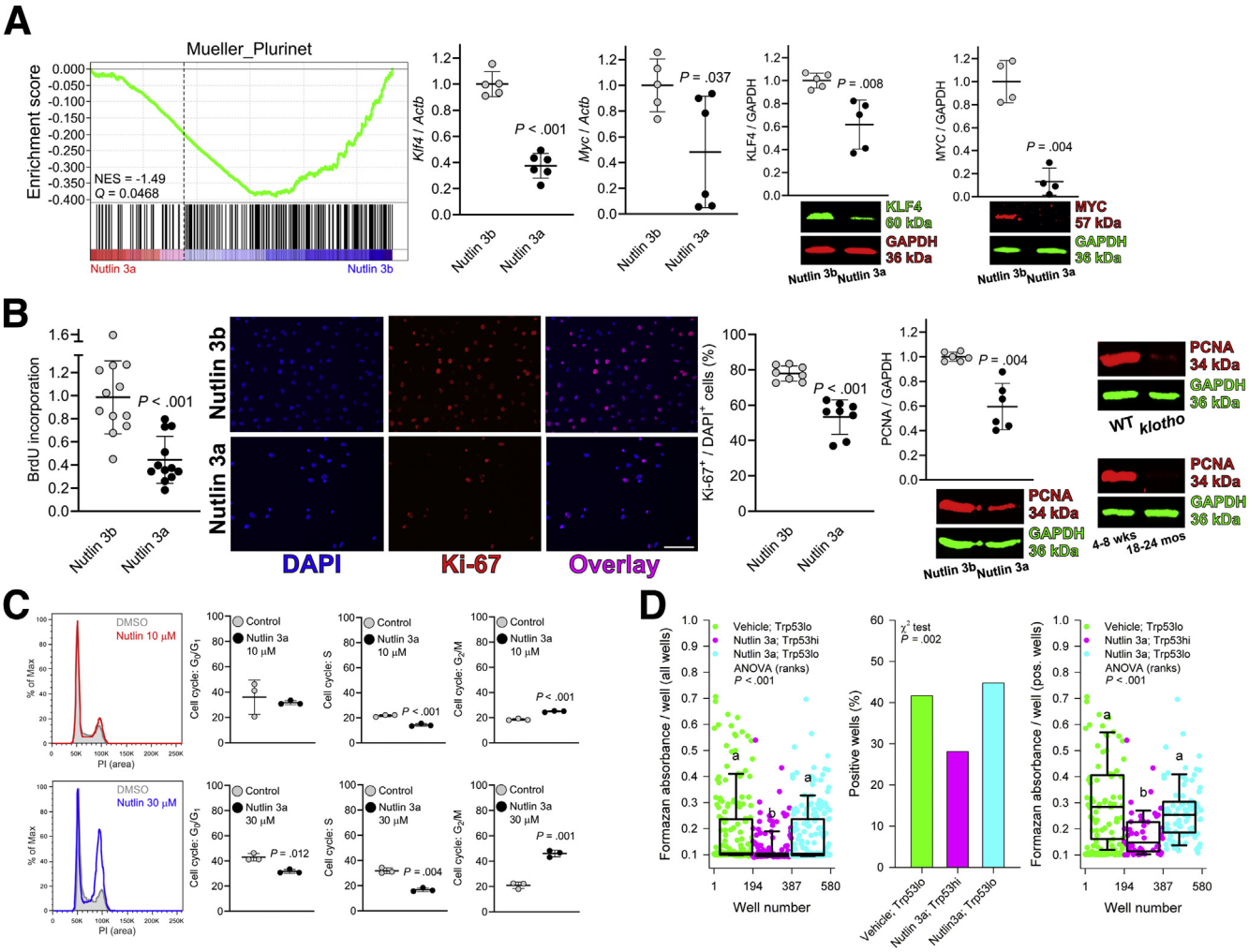

Figure 6. TRP53 activation inhibits ICC-SC growth by reducing cell proliferation and clonogenicity via down-regulation of self-renewal genes and cell cycle arrest. (*A*) *Left panel:* GSEA of total RNA-seq data showing down-regulation of stemness-related genes in D2211B ICC-SC treated with nutlin 3a vs cells treated with nutlin 3b (30 μmol/L, 72 hours; n = 3/group). *Vertical lines* indicate genes ranked by signal-to-noise ratios. Negative NES and FDR $Q < 0.25$ indicate significant depletion in nutlin 3a–treated group. See all data and gene sets analyzed in Table 4 and Supplementary Table 2. *Right panels:* reduced mRNA and protein levels of stemness genes KLF4 and MYC. *P* values are from Mann-Whitney rank sum tests. (*B*) Nutlin 3a (30 μmol/L, 72 hours) reduced D2211B proliferation by BrdU incorporation (n = 12/group), Ki-67 immunofluorescence (n = 10/group), and PCNA protein expression (n = 8/group). PCNA expression was also reduced in *klotho* and old mice vs their respective controls (n = 6/group). *P* values are from Mann-Whitney rank sum tests. (*C*) Cell cycle arrest detected by PI flow cytometric assay in D2211B cells treated with 30 μmol/L or 10 μmol/L nutlin 3a for 72 hours (n = 3/group). *P* values are from *t* tests applied to arcsine square root transformed data. (*D*) Nutlin 3a–treated (10 μmol/L, 3 days), clonally sorted, TRP53^{high} 2xSCS2F10 ICC-SC lentivirally transduced with the pGreenFire-p53-mCMV-EF1α-Puro Transcriptional Reporter displayed reduced clonogenicity and proliferation by MTS assay than vehicle-treated or nutlin 3a–treated, TRP53^{low} cells (192 wells/group). In the *left and right panels*, *P* values are from Kruskal-Wallis one-way ANOVA (ANOVA on ranks). Groups not sharing the same superscript are different by multiple comparisons (*left panel*, $P < .05$, Tukey tests; *right panel*, $P < .05$, Dunn's method). Proportions in the *middle panel* were analyzed by χ^2 test. PCNA, proliferating cell nuclear antigen.

WB analysis (Figure 5*D*), and immunofluorescent microscopy only revealed increased CL.CASP3 levels in the gastric mucosa but not in the tunica muscularis (Figure 5*E*). Together, these findings suggest no significant involvement of apoptosis and autophagy or canonical markers/mediators of cellular senescence or quiescence in gastric ICC-SC depletion with age.

However, the best definition of a senescent cell is an essentially permanent growth arrest, because molecular senescence markers are neither exclusive to this state nor universally applicable to different cell types.[18] Therefore, we next analyzed the effects of TRP53 induction on ICC-SC proliferation and the persistence of these effects in the absence of the initiating stimulus. GSEA of total RNA-seq data revealed depletion of stemness-related gene sets in nutlin 3a–treated D2211B cells (Figure 6*A*, Table 4, Supplementary Table 2). Kruppel-like factor 4 (KLF4) and myelocytomatosis oncogene (MYC), stemness genes

consistently expressed by ICC-SC, were reduced by RT-qPCR and WB (Figure 6*A*). MetaCore Biological Process Network Analysis of differentially expressed genes (Supplementary Dataset 2) indicated a predominance of cell cycle-related gene networks (G_1/S and G_2/M; Supplementary Dataset 3). We also detected significant reduction in the incorporation of the halogenated deoxyribonucleoside 5-bromo-2-deoxyuridine (BrdU), Ki-67 immunolabeling, and the expression of proliferating cell nuclear antigen (a protein associated with the DNA replication fork), which was also down-regulated in both *klotho* and aged mice (Figure 6B). Cell cycle analysis by propidium iodide (PI) flow cytometry in D2211B cells treated with 30 μmol/L nutlin 3a revealed arrest in the G_2/M phase with concomitant reduction of cells in G_0/G_1 and S phases (Figure 6*C*). In contrast, in response to 10 μmol/L nutlin 3a, a reduced proportion of cells in the S phase was the most prominent change. Collectively, these findings indicate that TRP53 activation reproduces Wnt-induced ICC-SC loss by down-regulating self-renewal genes and causing cell cycle arrest. To examine the persistence of these effects, we analyzed clonal growth in 2xSCS2F10 ICC-SC lentivirally transduced with the pGreenFire-p53-mCMV-EF1α-Puro Transcriptional Reporter and sorted singly into 96-well plates after 3 days of treatment with 10 μmol/L nutlin 3a or vehicle. After an additional 14 days of culturing in the absence of the drug, previously nutlin 3a–treated cells displaying high levels of TRP53-induced fluorescence showed significantly reduced clonogenicity as indicated by fewer positive wells and significantly lower level of methyltetrazolium salt (MTS) signal per well than vehicle-treated or nutlin 3a–treated cells with low or no reporter fluorescence (Figure 6*D*). Thus, even short-term (3-day) up-regulation of TRP53 increased the proportion of cells that lacked the ability to proliferate and also reduced the proliferative capacity of the cells that did not undergo cell cycle arrest likely because of some degree of stress relief.[17]

Transformation Related Protein 53 Inhibits Interstitial Cell of Cajal Stem Cell Proliferation via the ERK-CDKN1B-CCND1 Pathway

We next investigated the mechanisms that may underlie the TRP53-induced inhibition of S phase entry, because this mechanism, which is directly regulated by mitogen-activated protein kinases,[48] may be more conducive to future pharmacologic targeting than G_2/M arrest. Progression through G_1 and entry into S phase require the induction, in mid-G_1 phase, of cyclin D1 (CCND1) by extracellular signal-regulated mitogen-activated protein kinases ERK1 and ERK2. Formation of the CCND1-CDK4/6 (cyclin-dependent kinase 4/6) complex results in the sequestration of cyclin-dependent kinase inhibitors CDKN1A and CDKN1B ($p27^{Kip1}$), leading to the activation of cyclin E/A-CDK2 complexes and further cell cycle progression including S phase entry.[48] The predominantly transcriptionally controlled cyclin A/E-CDK2 inhibitor *Cdkn1a* was up-regulated by nutlin 3a in D2211B ICC-SC and *klotho* mice but increased only moderately in aged mice (Figure 4D). In nutlin 3a–treated D2211B ICC-SC, we also detected up-regulation of CDKN1B and down-regulation of CCND1, and phosphorylation of ERK1/2, a critical signaling mechanism for ICC survival and maintenance,[35,49] was reduced (Figure 7*A*). The same changes were also evident in the gastric muscles of *klotho* vs WT and old vs young mice (Figure 7*B*), as well as in 49- and 51-year-old patients vs 19- and 23-year-old controls (Figure 7*C*). Treatment with selumetinib (72 hours), a selective inhibitor of ERK1/2 phosphorylation, dose-dependently inhibited ERK1/2 phosphorylation, reduced CCND1 protein, up-regulated CDKN1B protein, and reduced ICC-SC viability (Figure 8*A* and *B*). ERK1/2 may facilitate the proteasomal degradation of CDKN1B directly or indirectly via up-regulation of CCND1.[48] To investigate the contribution of CDKN1B to TRP53-mediated inhibition of ICC-SC viability, we performed siRNA-mediated knockdown of *Cdkn1b* in D2211B cells in the presence of 30 μmol/L nutlin 3a or nutlin 3b. These experiments showed a significant, albeit modest, mitigation of nutlin 3a–induced reduction in ICC-SC viability by *Cdkn1b* siRNAs (Figure 8*C*). These results indicate that inhibition of the ERK-CDKN1B-CCND1 pathway also contributes to Wnt/TRP53-mediated ICC-SC depletion in aging (Figure 8*D*).

Discussion

ICC depletion is a prominent feature of gastrointestinal aging in humans.[15] In *klotho* mice, we previously linked gastric ICC loss to a decline in ICC-SC and impaired nitrergic neuromuscular neurotransmission.[11] Here, we generalized these observations by demonstrating similarly reduced ICC and ICC-SC and impaired compliance in the stomach of aged and *klotho* mice and by showing that the decline of ICC-SC precedes that of ICC, reflecting reduced ICC-SC proliferation. Furthermore, we offer a mechanistic explanation for the age-related depletion of the ICC lineage (Figure 8*D*). Our results support a role for overactive canonical Wnt signaling, possibly arising from reduced levels of the Wnt chaperone protein Klotho,[28] and TRP53 in the inhibition of ICC-SC self-renewal. Up-regulated canonical Wnt signaling from genetic loss of the Wnt inhibitor protein APC led to gastric ICC depletion in mice, providing in vivo validation of our concept. Downstream of TRP53, we detected repression of stemness genes, G_2/M arrest, and ERK inhibition causing G_1/S transition block via increased CDKN1B protein levels and down-regulation of CCND1. Three-day up-regulation of TRP53 in cultured ICC-SC led to persistent growth arrest without activating apoptosis, autophagy, cellular quiescence, or, surprisingly, canonical markers/mediators of cellular senescence. We have confirmed our key findings by studying *klotho* and aged mice and gastric tunica muscularis tissues from middle-aged humans.

Reduced protein consumption, likely from lower overall food intake,[3] has been linked to frailty and increased overall and cancer mortality in the elderly.[6] This anorexia of aging[3] may arise from early satiety and increased satiation reflecting reduced fundal compliance.[3–5] Previous work from our group established that ICC steadily decline at a

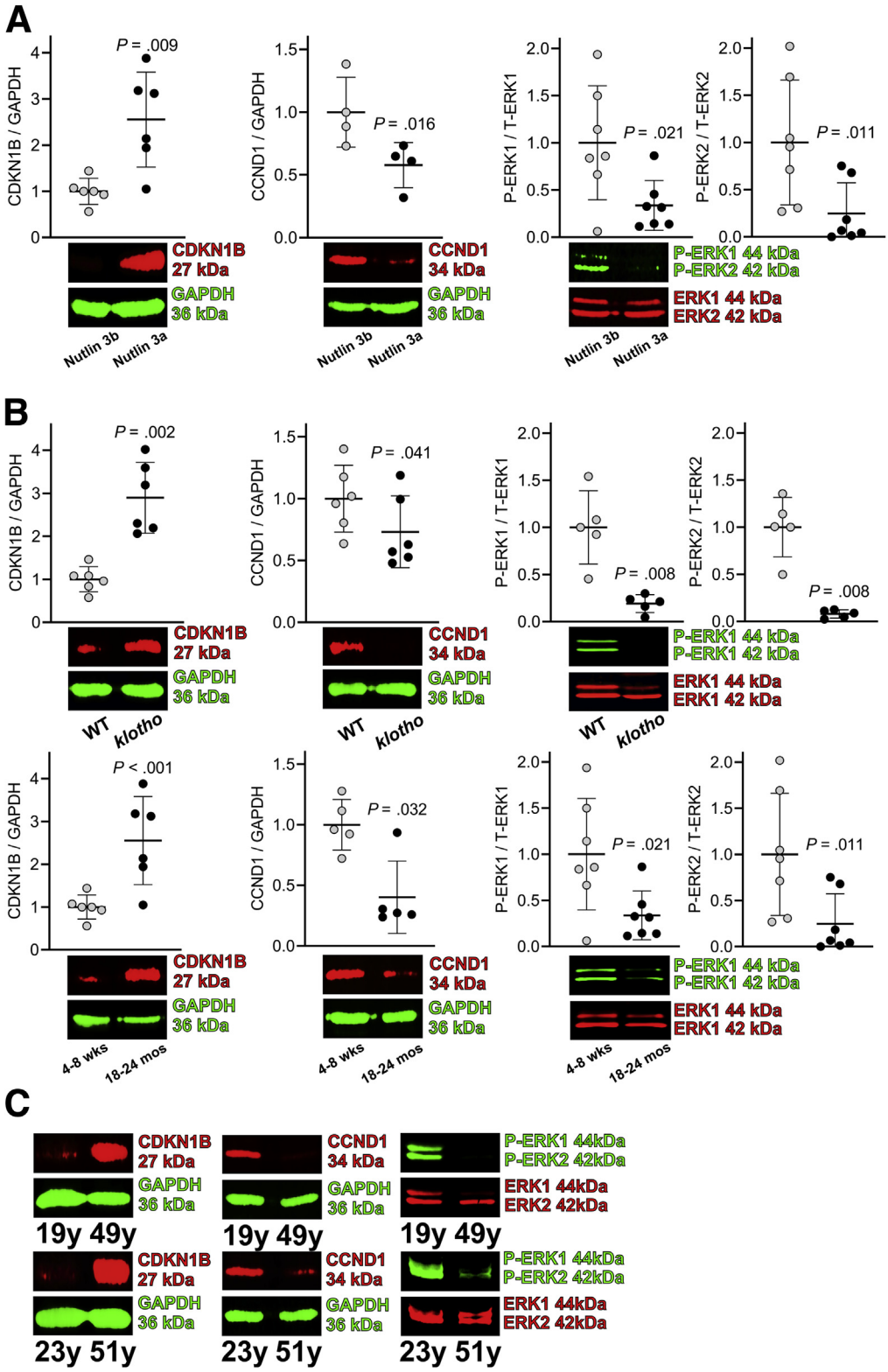

Figure 7. Increased CDKN1B, reduced CCND1, and reduced ERK activation in nutlin 3a–treated ICC-SC and during aging. (*A*) Nutlin 3a treatment (30 μmol/L, 72 hours) in D2211B cells up-regulated CDKN1B protein levels, down-regulated CCND1 protein levels, and reduced ERK1/2 phosphorylation by WB (n = 4–7/group). *P* values are from Mann-Whitney rank sum tests. (*B*) Increased CDKN1B protein, reduced CCND1 protein, and reduced ERK1/2 phosphorylation in *klotho* mouse gastric lysates compared with WT controls and in old vs young mice (n = 5–8/group). *P* values are from Mann-Whitney rank sum tests. (*C*) Up-regulated CDKN1B protein, reduced CCDN1 protein, and reduced ERK1/2 phosphorylation in the gastric corpus muscles of 49-year-old and 51-year-old patients vs 19-year-old and 23-year-old controls.

rate of ~13% per decade of adult human life.[15] Consistent with a role for this age-related ICC loss in anorexia of aging, in *klotho* mice we previously reported net caloric deficit accompanying impaired nitrergic neuromuscular neurotransmission from ICC depletion,[11] and in KIT ligand-deficient Sl/Sl^d mice, primary loss of intramuscular ICC was associated with early satiation, decreased meal size, and reduced body weight.[50] ICC populations likely have a

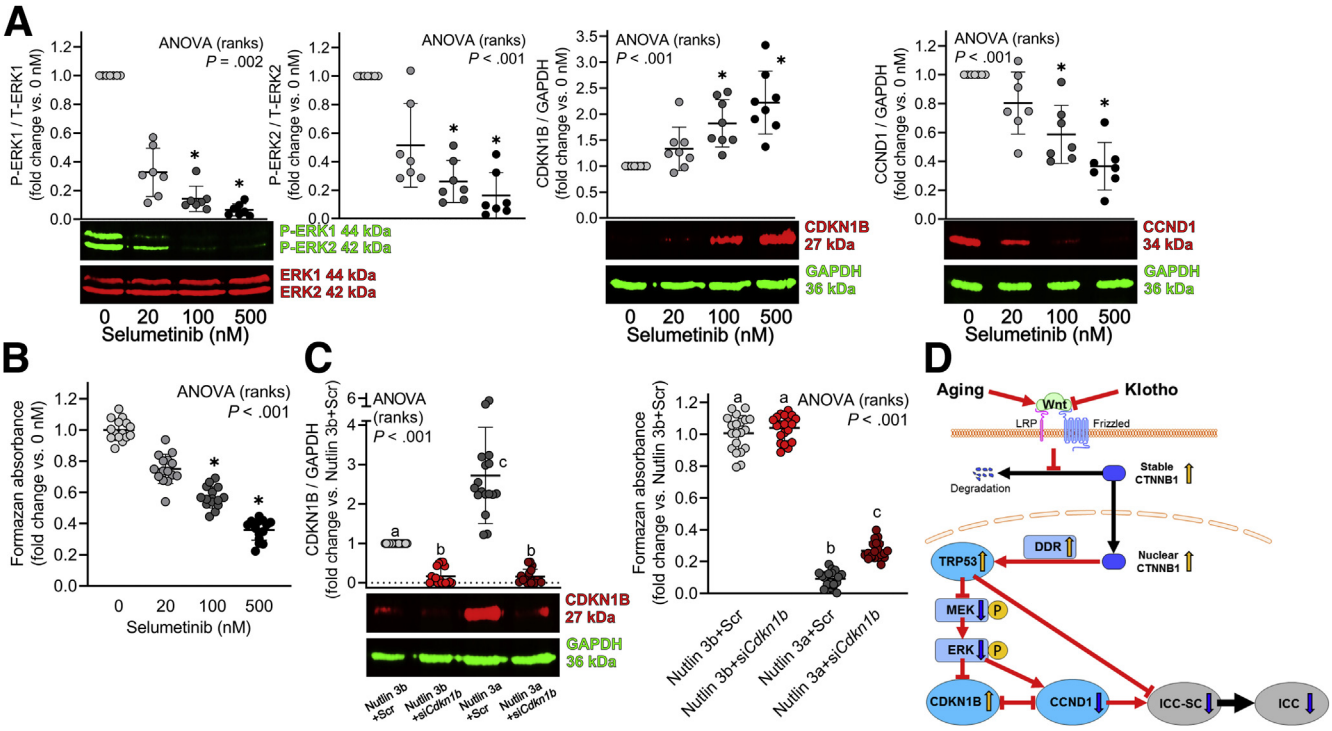

Figure 8. TRP53 inhibits ICC-SC proliferation via the ERK-CDKN1B-CCND1 pathway. (*A*) The mitogen-activated protein kinase kinase 1/2 (MEK1/2) inhibitor selumetinib applied for 3 days dose-dependently reduced ERK phosphorylation, increased CDKN1B protein levels, and reduced CCND1 protein by WB (n = 7–8/group) in D2211B ICC-SC. *P* values are from Kruskal-Wallis one-way ANOVA (ANOVA on ranks). **P* < .05 vs vehicle control by post hoc multiple comparisons (Dunn's method). (*B*) Selumetinib also dose-dependently inhibited ICC-SC viability by MTS assay (n = 15/group). *P* value is from Kruskal-Wallis one-way ANOVA (ANOVA on ranks). **P* < .05 vs vehicle control by post hoc multiple comparisons (Dunn's method). (*C*) siRNA-mediated knockdown of *Cdkn1b*, verified by WB, mitigated the nutlin 3a–induced reduction in D2211B growth by MTS assay (n = 20/group). *P* values are from Kruskal-Wallis one-way ANOVA (ANOVA on ranks). Groups not sharing the same superscript are different by multiple comparisons (*P* < .05, Tukey tests). (*D*) Proposed mechanisms of ICC-SC depletion leading to ICC loss during aging. Aging causes overactive Wnt signaling in part by reducing Klotho protein levels. Increased Wnt signaling increases TRP53 protein levels by stabilizing CTNNB1 and promoting its nuclear localization and by inducing DDR. TRP53 causes ICC depletion in part by inhibiting ICC-SC proliferation via G_2/M arrest. TRP53 also inhibits ERK1/2 phosphorylation (P), decreasing CCND1 and increasing CDKN1B protein levels. Reduced CCND1, likely together with other G_1/S cyclins, down-regulates ICC-SC proliferation and self-renewal by interfering with S phase entry.

significant reserve because a more subtle—but, as our present data confirm, clearly detectable—decline in middle-aged individuals does not appear to result in a frank decrease in food intake. Whether the more modest ICC loss could still reduce ability to maintain nutritional status in response to metabolic challenge associated with various diseases remains unclear and will require further clinical studies.

In this study, we extended our previous finding of ICC loss-associated impaired nitrergic neuromuscular neurotransmission[11] to the organ level by demonstrating impaired ex vivo gastric compliance in both *klotho* and naturally aged mice. Reduced compliance has also been reported in excised guinea pig stomachs and in anesthetized rats after exposure to nitric oxide synthesis inhibitors,[51,52] supporting the notion that impaired compliance in our models reflected reduced nitrergic signaling. However, in isolated mouse stomachs, the same type of pharmacologic intervention appeared to increase compliance,[53] a finding that remains mechanistically unexplained. Also, in the rat stomach, nitrergic relaxation in response to distention was vagally mediated,[52] whereas we focused on local reflexes because our approach did not permit the assessment of vagal mechanisms. Because vagal intramuscular arrays, which are structures presumed to function as stretch receptors,[9] have been shown to make extensive synapse-like connections with intramuscular ICC throughout the stomach,[9] age-related ICC loss may also impair vagovagal reflexes that contribute to distention-induced relaxation. This intriguing possibility requires further investigation.

The results from our current and previous study[11] indicate that the main physiological consequence of aging-associated ICC loss is impaired gastric compliance due to reduced nitrergic neuromuscular neurotransmission. However, ICC also mediate cholinergic excitatory mechanisms.[14] Although it is possible that a more subtle decline in cholinergic excitation was masked by a more robustly impaired nitrergic relaxation, our previous electrophysiological and pharmacologic studies in the *klotho* stomach did not reveal a reduction in cholinergic responses,[11] and

neither we nor Phillips et al[8] found a significant change in either nitrergic or total neurons in the stomach of *klotho* mice and aged rats, respectively. Therefore, at the present time we are unable to explain why nitrergic inhibitory neuromuscular signaling is selectively affected in our models showing age-related ICC depletion.

Klotho protein levels are reduced during aging. Klotho mitigates/delays stem cell senescence by binding to Wnt family members.[16,28] On the basis of the pronounced depletion of the ICC lineage in *klotho* mice hypomorphic for Klotho,[11] we hypothesized that overactive Wnt signaling may also underlie age-related ICC loss, and TRP53, a major target of Wnt/CTNNB1 signaling in murine embryonic stem cells,[54] may mediate this effect. By using multiple, orthogonal approaches of transcriptome analysis, immunohistochemistry, Wnt3a treatments, overexpression of constitutively active CTNNB1, and studying mice deficient in the Wnt signaling inhibitor APC, we established a role for canonical Wnt signaling in the ICC lineage and showed that its activation can both stimulate and, after prolonged exposure, inhibit ICC-SC proliferation. Overactive canonical Wnt signaling was clearly demonstrable in the gastric musculature of *klotho* and aged mice and middle-aged humans and associated with DDR and TRP53 up-regulation. These effects could be reproduced by pharmacologic stabilization of TRP53 and linked to G_2/M and ERK-CDKN1B-CCND1–mediated G_1/S transition blockade occurring without activation of apoptosis, autophagy, or cellular quiescence pathways. Although TRP53 activation caused persistent cell cycle arrest, we found no convincing evidence of up-regulation of canonical markers/mediators of cellular senescence. At the present time, we cannot explain this finding. A limitation of our study is that the D2211B and 2xSCS70 cell lines were originally isolated from mice expressing a temperature-sensitive mutant SV40 tsTAg. However, both lines have been maintained in the verified absence of tsTAg,[21] whose effects on senescence are readily reversible.[46] Furthermore, the 2xSCS2F10 ICC-SC line also used in this study is from WT (C57BL/6) mice,[21] and we found no evidence of up-regulation of SA-β-gal,[17,18,47] the most widely used senescence marker, in the gastric tunica muscularis of *klotho* or aged mice. Therefore, considering that molecular senescence markers are neither exclusive to this state nor universally applicable to different cell types,[18] we propose that in the gastrointestinal tunica muscularis, persistent cell cycle arrest and other aspects of cellular senescence may be mediated by mechanisms different from those observed in the rapidly proliferating cells of the mucosa and other tissues. Identification of these mechanisms and associated biomarkers will require further studies.

Reduced proliferative capacity of ICC-SC can be expected to lead to diminished pools of both ICC-SC and ICC because the latter require constant replacement because of natural attrition.[11,15,20,37] Indeed, age-dependent stem cell depletion from reduced self-renewal has been reported in skeletal muscle, neural, and germline stem cells.[55] However, ICC-SC and ICC frequencies ran approximately parallel courses during both the period of initial rapid decline of ICC, which by lineage tracing we previously attributed to a combined effect of ICC transdifferentiation and death,[37] and their subsequent stabilization. These results suggest that changes in the demand for ICC replacement may ultimately determine the rate of ICC-SC loss through the regulation of the speed of ICC-SC self-renewal and resultant exhaustion. This proposed mechanism is consistent with the effects of increased Wnt signaling on other stem cell types.[26–28,55] However, the signals communicating the size of the ICC pool to the ICC-SC remain to be identified. It is also important to note that ICC at some stages of maturity may also be able to proliferate.[56] Indeed, we counted very similar numbers of EdU^+ cells among ICC-SC and ICC after daily administration of this labeled nucleoside for 2 weeks. However, EdU^+ ICC-SC were more consistently reduced in *klotho* mice, and the EdU^+ cells represented $\sim$9 times greater percentage of ICC-SC than ICC populations. These findings suggest that at least a part of the EdU^+ ICC may have originally been labeled as ICC-SC during the early days of the EdU treatment regimen. Further studies using a pulse-chase paradigm[37] are needed to fully understand the dynamic aspects of ICC differentiation from their precursors.

In conclusion, our findings identify a novel role for canonical Wnt signaling in ICC-SC proliferation and establish a link between overactive Wnt signaling, TRP53 activation, and persistent cell cycle arrest in aging-associated ICC-SC and ICC depletion. Age-related ICC loss leads to gastric dysfunction predominantly by impairing gastric compliance through reducing nitrergic neuromuscular neurotransmission, as we demonstrated previously.[11] Age-related ICC-SC/ICC depletion could potentially be countered by the inhibition of the Wnt/CTNNB1 and/or stimulation of ERK-mediated signaling pathways.

Materials

Recombinant mouse Wnt3a was from Calbiochem (EMD Millipore, Billerica, MA). Nutlin 3a and nutlin 3b were from Cayman Chemical (Ann Arbor, MI). Dimethyl sulfoxide (DMSO), Staurosporin, and Triton-X were from Sigma-Aldrich (St Louis, MO). Selumetinib (AZD6244) was from Selleckchem (Houston, TX).

Animal Experiments

Homozygous *klotho* mice hypomorphic for α-Klotho and age-matched WT littermates (both sexes) were obtained from our heterozygous breeders, and their genotype was verified by PCR as reported previously.[11,12,16] Experiments were performed between 50 and 70 days of age. At 4–5 weeks of age, *klotho* and WT mice were intraperitoneally injected with EdU (50 mg/kg body weight) for 2 weeks to label proliferating cells. $APC^{\Delta 468}$ mice with overactivated CTNNB1 signaling due to disruption of the *Apc* gene were developed by Khazaie and colleagues.[34] The 5-month-old $APC^{\Delta 468}$ mice and age-matched WT mice (both sexes) were used after the verification of their genotype as described previously.[34] WT controls for genetically modified mice were co-housed

with their mutant siblings. Male 18- to 24-month-old C57BL/6 mice were from the National Institute on Aging (Bethesda, MD). One- to 107-week-old WT mice of C57BL/6 or BALB/c background and of either sex were from Charles River Laboratories (Wilmington, MA), the Jackson Laboratory (Bar Harbor, ME), and our colonies. None of the mice were used in any previous experiments.

Mice were housed maximum 5/cage using an Allentown, Inc (Allentown, NJ) reusable static caging system in the Mayo Clinic Department of Comparative Medicine Guggenheim Vivarium under a 12-hour light/12-hour dark cycle. Bedding material was irradiated one-fourth-inch corn cob with the addition of Bed-r'Nest (4 g; The Andersons, Inc, Maumee, OH) irradiated paper-twist nesting material as enrichment. Mice were kept on irradiated PicoLab 5058 Mouse Diet 20 ($\geq$20% protein, $\geq$9% fat, $\leq$4% fiber, $\leq$6.5% ash, $\leq$12% moisture; LabDiet, Inc, St Louis, MO). Food and water were available ad libitum. Before gastric compliance studies, mice were fasted overnight in a metabolic cage with free access to water. Animals were handled during the light phase.

Mice were killed by CO_2 inhalation anesthesia or by decapitation performed under deep isoflurane (Baxter Healthcare, Deerfield, IL) inhalation anesthesia.

Tissues and Cell Lines

Gastric corpus + antrum muscles were prepared as described.[20] Pieces of human gastric corpus tunica muscularis were prepared by cutting away the mucosa and submucosa. Isolation and maintenance of the ICC-SC cell lines D2211B, 2xSCS70, and 2xSCS2F10 were described previously.[21] Only cells with diploid DNA content and lacking expression of the temperature-sensitive tsTAg were used.[21]

Gastric Compliance

Ex vivo gastric compliance was determined according to previously described approaches[51–53] with minor modifications. Briefly, intact stomachs were excised, placed in a heated water bath, and connected via the esophagus to a syringe pump (Model 975 Compact Infusion Pump; Harvard Apparatus, Ltd, Cambridge, MA) and a pressure transducer (MP100A-CE; BIOPAC Systems, Inc, Goleta, CA; amplifier: Transbridge 4M; World Precision Instruments, Sarasota, FL) through the pylorus. The stomachs were then filled with Krebs solution[36] (37°C) to 1 mL at a rate of 100 μL/min while recording pressure using ClampFit 10.7.0 software (Molecular Devices, LLC, San Jose, CA).

Western Immunoblotting

Tissue and cell lysates were prepared and subjected to sodium dodecyl sulfate–polyacrylamide gel electrophoresis and immunoblotting as described previously[57] (antibodies in Table 6). Target and reference proteins were detected simultaneously by using LI-COR Biosciences (Lincoln, NE) secondary antibodies tagged with near-infrared and infrared fluorescent dyes (IRDye700, red pseudocolor; IRDye800CW, green pseudocolor). For nuclear β-catenin detection, nuclear faction was isolated according to manufacturer's instruction (EMD Millipore).

Multiparameter Flow Cytometry

Murine gastric $KIT^{+}CD44^{+}CD34^{-}$ ICC and $KIT^{low}CD44^{+}CD34^{+}$ ICC-SC were enumerated by using previously published protocols and reagents[20,21] (Tables 7 and 8). EdU^{+} proliferating in ICC-SC and ICC were detected by Click-iT Plus EdU Alexa Fluor 488 Flow Cytometry Assay Kit (Thermo Fisher Scientific, Waltham, MA) according to the manufacturer's protocol (see details under Cell cycle analysis)

Transcriptome Analysis by Total Stranded RNA Sequencing

Total RNA was isolated from nutlin 3a– and nutlin 3b–treated D2211B cells and purified by using the Qiagen (Valencia, CA) RNeasy Mini Kit. Sequencing libraries were constructed by using 100 ng total RNA and the TruSeq Stranded Total RNA LT (with Ribo-Zero Human/Mouse/Rat) Set A kit (Illumina, San Diego, CA). Libraries were sequenced at 60–110 million fragment reads per sample following Illumina's standard protocol using the Illumina cBot and HiSeq 3000/4000 PE Cluster Kit. The flow cells were sequenced as 101 $\times$ 2 paired-end reads on an Illumina HiSeq 4000 using HiSeq 3000/4000 SBS Kit (150 cycles) and HCS v 3.3.52 collection software. Base-calling was performed using Illumina's RTA version 2.7.3. The transcriptome data have been deposited in a public database (National Center for Biotechnology Information, U.S. National Library of Medicine Gene Expression Omnibus (GEO), https://www.ncbi.nlm.nih.gov/gds/) as series GSE139539.

Transcriptome Data Analysis

Raw total RNA-seq data generated for this study or downloaded from GEO (https://www.ncbi.nlm.nih.gov/gds/; datasets GSE60853[22] and GSE57776[38]) were analyzed by the MAP-RSeq 3.0.1 pipeline developed by the Mayo Clinic Bioinformatics Core.[58] Briefly, the pipeline generates detailed quality control data to estimate the distance between paired-end reads, evaluate the sequencing depth for alternate splicing analysis, determine the rate of duplicate reads, and to evaluate coverage of reads across genes by using the RSeQC software.[59] Paired-end reads were aligned to the mouse genome (mm10) using the Spliced Transcripts Alignment to a Reference software package.[60] Gene and exon counts were generated by using HTseq software (http://www-huber.embl.de/users/anders/HTSeq/doc/overview.html). Gene annotation files were obtained from Illumina (http://cufflinks.cbcb.umd.edu/igenomes.html). Differential gene expression between nutlin 3a– and nutlin 3b–treated cells was analyzed by using the Bioconductor package edgeR.[61] Differentially expressed genes (Benjamini-Hochberg false discovery rate [FDR] $Q < 0.05$) were analyzed for biological process networks by using MetaCore software. Biological process network analysis was also applied to the average reads per kilobase of transcript per million mapped reads (RPKM) (gene count) values obtained for the individual ICC classes and ICC-SC cell lines.

Table 6. Antibodies Used in WB Studies

Target	Supplier	Host	Clone/ID	Isotype/lot #	Label	Final concentration
GAPDH	Imgenex[a]	Goat pAb	IMG-3073			0.05 μg/mL
GAPDH	Sigma[b]	Rabbit pAb	G9545			1:40,000
ANO1	Abcam[c]	Rabbit pAb	Ab53512	GR71118-2		0.2 μg/mL
CDKN1B	BD	Mouse mAb	57/Kip1/p27	IgG_1		0.125 μg/ml
Cleaved caspase 3	CST[d]	Rabbit pAb	9661	42		1:1000
CTNNB1	BD	Mouse mAb	14/Beta-catenin	IgG_1		0.016 μg/mL
CTNNB1	CST	Rabbit mAb	9582	IgG		1:2000
CCND1	CST	Rabbit pAb	2922	3		1:1000
C-MYC	CST	Rabbit pAb	5605	IgG		1:2000
ERK1/2	CST	Mouse mAb	3A7	IgG_1		1:4000
ETV1	Abcam	Rabbit pAb	Ab81086	GR12174-15		0.5 μg/mL
H3	CST	Rabbit pAb	2650	TF268338		1:2000
LC3B	CST	Rabbit pAb	2775	5		1:2000
KLF4	RDS	Goat pAb	AF3158	WPR0208121		0.2 μg/mL
KIT	Dako[e]	Rabbit pAb	A4502	10042820A		1:4000
KIT	RDS[f]	Goat pAb	AF1356	IEO0211011		0.2 μg/mL
PCNA	CST	Mouse mAb	2586	IgG_{2a}		1:2000
P-CTNNB1 (Ser33/37/Thr41)	CST	Rabbit pAb	9561	10		1:2000
P-ERK1/2 (202Y204 and T185/T187)	CST	Rabbit mAb	197G2	IgG		1:1500
TRP53	CST	Mouse mAb	1C12	$IgG_{1\kappa}$		1:2000
Secondary Ab: anti-rabbit IgG (H+L)	LI-COR[g]	Donkey pAb	#926-32223	C90821-03	IRDye 680	1:10,000
Secondary Ab: anti-mouse IgG (H+L)	LI-COR	Donkey pAb	#926-32222	C71204-03	IRDye 680	1:10,000
Secondary Ab: anti-rabbit IgG (H+L)	LI-COR	Donkey pAb	#926-32213	C70918-03	IRDye 800CW	1:10,000
Secondary Ab: anti-goat IgG (H+L)	LI-COR	Donkey pAb	#926-32214	C80207-07	IRDye 800CW	1:10,000

Ab, antibody; H+L, highly cross-adsorbed; Ig, immunoglobulin; mAB, monoclonal antibody; pAb, polyclonal antibody.
[a]Imgenex Corp, San Diego, CA.
[b]Sigma-Aldrich, Inc, St Louis, MO
[c]Abcam plc, Cambridge, MA.
[d]CST; Cell Signaling Technology, Inc, Beverly, MA.
[e]Dako North America, Inc, Carpinteria, CA.
[f]R&D Systems, Inc, Minneapolis, MN.
[g]LI-COR Biosciences, Lincoln, NE.

Previously published transcriptome data generated by using Affymetrix Mouse Genome 430 2.0 Arrays (MG430.2) (GEO gene sets GSE7809[39] and GSE60744[22]) and Affymetrix Human Genome U133 Plus 2.0 Arrays (HGU133+2) (GEO gene set GSE77839[40]) were analyzed as described in the original publications.[22,39,40] Briefly, probe-level data were pre-processed by robust multiple-array analysis and analyzed for differential gene expression vs unfractionated tunica muscularis source tissues by the empirical Bayes approach with Benjamini-Hochberg adjustment using software packages in Bioconductor.[39] Differentially up-regulated genes ($Q < 0.05$ AND $\log_2 FC > 1$) were subjected to MetaCore biological process network analysis.

Differential enrichment of gene sets assembled into matrices was determined by GSEA (https://www.gsea-msigdb.org/gsea/index.jsp)[41] applied to the normalized gene expression values (RPKM). Average RPKM data from individual cell types or cell lines were subjected to GSEA Preranked analysis. The gene set matrices interrogated were assembled by searching the Molecular Signatures Database (MSigDB) 6.2[41] for the terms specified in the footnotes to Tables 2–5. Genes assigned to the indicated gene sets are listed in Supplementary Tables 1–4. Both the standard (differential) and Preranked GSEA analyses were performed by using default parameters. Tables 2–5 list the number of genes in the datasets that belong to the individual gene sets (size), the normalized enrichment score (NES), and the FDR Q value (cutoff for significance, 0.25).[41]

Immunohistochemistry and Fluorescent Microscopy

Mouse gastric tissues were fixed with 4% paraformaldehyde for 2 hours at 4°C or with cold acetone (10 minutes). Five-μm cryosections were blocked with 1% bovine serum albumin (Sigma-Aldrich), incubated with primary antibodies (Table 9) at 4°C overnight, washed, and

Table 7. Antibodies Used for Flow Cytometry Analysis of Cells Freshly Dissociated From Murine Gastric Muscles

Target	Supplier	Host/Source	Clone/ID	Isotype	Label	Final concentration or μg/10^6 cells[a]
CD16/32[b]	eBioscience	Rat mc	93	IgG2a, λ		1 μg
CD11b[c]	eBioscience	Rat mc	M1/70	IgG_{2b}, κ	PE-Cy7	0.0312 μg
CD45[d]	eBioscience	Rat mc	30-F11	IgG_{2b}, κ	PE-Cy7	0.0312 μg
F4/80[e]	eBioscience	Rat mc	BM8	IgG_{2a}, κ	PE-Cy7	0.0625 μg
CD44[f]	BioLegend	Rat mc	IM7	IgG_{2b}, κ	APC-Cy7	0.0625 μg
KIT	eBioscience	Rat mc	ACK2	IgG_{2b}, κ	APC	5 μg/mL
KIT	eBioscience	Rat mc	2B8	IgG_{2b}, κ	APC	0.25 μg
CD34[g]	eBioscience	Rat mc	RAM34	IgG_{2a}, κ	eFluor 450 or FITC	0.2 μg

NOTE. Suppliers: eBioscience, Inc, San Diego, CA; BioLegend, San Diego, CA.
Cy7, cyanine 7; FITC, fluorescein isothiocyanate; Ig, immunoglobulin; mc, monoclonal.
[a]Amount added to 100 μL of staining volume.
[b]CD16: Fc receptor, IgG, low affinity III; CD32: Fc receptor, IgG, low affinity IIb.
[c]CD11b, integrin alpha M.
[d]CD45, protein tyrosine phosphatase, receptor type, C.
[e]F4/80, epidermal growth factor–like module containing mucin-like, hormone receptor-like sequence 1.
[f]CD44 antigen.
[g]CD34 antigen.

incubated with fluorochrome-tagged secondary antibodies (Table 9) at room temperature for 30 minutes. Nuclei were counterstained with 4′,6-diamidino-2-phenylindole (DAPI). Wide-field fluorescence images of 5-μm cryosections were captured with either a Nikon (Melville, NY) Eclipse TS-100F microscope equipped with a Modulation Optics (Glen Cove, NY) HMC ELWD Plan Fluor 40×, 0.60 NA air objective and a Jenoptik (Brighton, MI) MFCool CCD camera or an Olympus (Center Valley, PA) Magnafire camera mounted on an Olympus BX51 microscope equipped with a UPlanFl 40×, 0.75 NA air objective. Specificity of immunolabeling was verified by omitting the primary antibodies and by examining the samples with filter sets not designed for the fluorochrome used.

Immunofluorescence Analysis of Cell Cultures

D2211B cells were plated onto no. 1 coverslips coated with rat-tail collagen and maintained with complete growth media. After Wnt3a or nutlin 3a treatment, the cells were washed, fixed with 4% paraformaldehyde for 10 minutes at room temperature, permeabilized with 0.3% Triton X-100 for 10 minutes at room temperature, and blocked with 1% bovine serum albumin in phosphate-buffered saline (pH 7.4) overnight at 4°C. After labeling with anti-Ki-67 or anti-γ-H2A.X antibodies (Table 9) at 4°C overnight, the cells were washed and incubated with fluorochrome-tagged secondary antibodies (Table 9) at room temperature for 30 minutes. Nuclei were counterstained with DAPI. Images were captured with a Nikon Eclipse TS-100F microscope

Table 8. Configuration of the Becton Dickinson LSR II Flow Cytometer

Laser	Excitation wavelength[36]	Dichroic filter[36]	Emission filter (*nm*; peak/bandwith)	Detector type	Light scatter or fluorochromes used
Coherent Sapphire, 20 mW	488			Photodiode	Forward scatter
			488/10	PMT	Side scatter
		505 LP	530/30	PMT	FITC, AF488
		550 LP	575/26	PMT	Unused
		595 LP	610/20	PMT	Unused
		685 LP	695/40	PMT	Beads
		735 LP	780/60	PMT	PE-Cy7
Coherent CUBE, 100 mW	407		450/50	PMT	eFluor 450
		505LP	525/50	PMT	Unused
		535 LP	590/40	PMT	Unused
		595 LP	610/20	PMT	Unused
		630 LP	670/30	PMT	Unused
		670 LP	710/50	PMT	Unused
Coherent CUBE, 40 mW	640		660/20	PMT	APC, AF647
		685 LP	712/20	PMT	Beads
		735 LP	780/60	PMT	APC-Cy7

AF, Alexa Fluor; Cy7, cyanine 7; FITC, fluorescein isothiocyanate; LP, long-pass; PMT, photomultiplier tube.

Table 9. Antibodies Used in the Mouse Immunohistochemistry and Immunocytochemistry Studies

Target	Supplier	Host	Clone/ID	Isotype/lot #	Label	Final concentration
Cleaved caspase 3	CST[a]	Rabbit pAb	9661	42		1:1000
CTNNB1	BD	Mouse mAb	14/Beta-catenin	IgG_1		0.5 μg/mL
γ-H2A.X (Ser139)	CST	Rabbit mAb	9718	IgG		1:400
Ki-67	CST	Rabbit mAb	D3B5	IgG		1:1000
KIT	House	Rat mAb	ACK2	$IgG_{2b\kappa}$		5 μg/mL (for whole mount)
KIT	Dako	Rabbit pAb	A4502	10042820A		1:200
Secondary Ab: anti-rat IgG	LT[b]	Goat pAb	A-11006	414662	AF488	5 μg/mL
Secondary Ab: anti-rat IgG	LT	Goat pAb	A-11008	1736968	AF488	5 μg/mL
Secondary Ab: anti-rabbit IgG	LT	Chicken pAb	A-21442	1694423	AF594	5 μg/mL
Secondary Ab: anti-mouse IgG	LT	Goat pAb	A-11005	10042820A	AF594	5 μg/mL

AF, Alexa Fluor; Ig, immunoglobulin; mAb, monoclonal antibody; pAb, polyclonal antibody.
[a]CST, Cell Signaling Technology, Inc, Beverly, MA.
[b]LT, Life Technologies, Grand Island, NY.

equipped with a Modulation Optics 20× HMC ELWD Plan Fluor 0.45 NA air objective and a Jenoptik ProgRes MFCool CCD camera.

Beta-Catenin Overexpression

In 2xSCS2F10 ICC-SC, overexpression of a constitutively active β-catenin mutant lacking the glycogen synthase kinase 3 phosphorylation sites required for proteasomal degradation (*Ctnnb1*ΔGSK-KT3; Addgene plasmid #14717, a gift from Tannishtha Reya[24]) was performed using Cell Line Nucleofector Kit L (Lonza, Allendale, NJ). The 10^6 2xSCS2F10 cells were resuspended in 100 μL nucleofector solution L. The 100 μL cell suspension was combined with 2 μg plasmid or 2 μg pmaxGFP vector used as control. Program T-030 was used for the electrical settings. Expression was verified by WB.

RNA Interference

Cdkn1b or *Ctnnb1* knockdown was performed by using Dhamacon ON-TARGETplus SMARTpool siRNA or corresponding scrambled sequences (25 nmol/L) and DharmaFECT1 Transfection Reagent (Thermo Fisher Scientific) according to the manufacturer's protocol. Treatment was applied after 1-day culturing in antibiotic-free and antimycotic-free media. Knockdown efficacy was assessed after 72 hours by WB.

Quantitative Reverse Transcription Polymerase Chain Reaction

RT-qPCR was performed by using previously published methods and specific, intron-spanning primers (Table 10).[62] The cDNA was amplified on a Bio-Rad CFX96 (Bio-Rad Life Science Research, Hercules, CA) real-time PCR detector using the SYBR GreenER qPCR SuperMix (Thermo Fisher Scientific).

Assay of Viable Cell Counts and Proliferation

Three thousand cells per well were plated in complete media in 96-well flat-bottom plates. After 72 hours, cells were incubated as indicated. Viable cell counts and

Table 10. RT-qPCR Primer Sequences

Gene symbol	Protein	Primer sequences
Klf4	Kruppel like factor 4	ATTATCAAGAGCTCATGCCACCG TTCTCGCCTGTGTGAGTTCGCA
Myc	C-MYC	ACAGCAGCTCGCCCAAATCCTGTA CTCTTCTTCAGAGTCGCTGCTGGT
Trp53	Transformation related protein 53 (TRP53)	TGTCATCTTTTGTCCCTTCTCA CAGCGTCTCACGACCTCC
Sesn2	Sestrin2	ACGGCGAGGTAAACCAGCTCC CCTTGCACAGAGGACGGTGGA
Sesn3	Sestrin3	TCGATACATTGAAGACCCAGCTTTGGG GGCCATTGTGTTGTAGGTGAGATTGT
Cdkn1a	Cyclin-dependent kinase inhibitor 1A (CDKN1A)	TTGCACTCTGGTGTCTGAGC CTGCGCTTGGAGTGATAGAA
Actb	Actin, beta	ATGGTGGGAATGGGTCAGAAGG GCTCATTGTAGAAGGTGTGGTGCC

proliferation were evaluated by MTS assay (CellTiter 96 AQ_{ueous} Non-Radioactive Cell Proliferation Assay; Promega, Madison, WI) and 5-bromo-2-deoxyuridine cell proliferation assay (Cell Signaling Technology, Danvers, MA), respectively.

Senescence-Associated β-Galactosidase Histochemistry

Gastric tissues from naturally aged mice and young mice as well as *klotho* and age- and sex-matched WT mice were fixed with 4% PFA for 2 hours at 4°C. SA-β-gal activity was detected in 5-μm cryosections of the stomachs by using SA-β-gal staining Kit (Cell Signaling Technology) following the manufacturer's protocol.

Cell Cycle Analysis

The Click-iT EdU Alexa Fluor (AF) 647 Flow Cytometry Assay Kit (Thermo Fisher Scientific) was used according to the manufacturer's protocol with minor modifications. Briefly, EdU was added to cell culture medium to a final concentration of 10 μmol/L for 60 minutes. After a wash, cells were harvested, pelleted at 500*g* for 5 minutes, and fixed for 15 minutes at room temperature with Click-iT fixative containing 4% paraformaldehyde. After washing and centrifugation, the cells were permeabilized with Click-iT saponin-based permeabilization buffer and incubated with 500 μL Click-iT reaction cocktail containing the AF 647 fluorochrome for 30 minutes at room temperature in the dark. After a wash with the Click-iT permeabilization buffer, the cells were incubated with 20 mg/mL ribonuclease A and PI staining solution (50 μg/mL) for 45 minutes at room temperature in the dark. Samples were analyzed by using a Becton Dickinson LSR II flow cytometer (Table 8 for configuration) and FlowJo software (Treestar, Woodburn, OR). Chicken erythrocyte nuclei (used for checking instrument linearity) and calf thymocyte nuclei (BioSure, Grass Valley, CA) were used as controls.

Clonogenicity Assay

The 2xSCS2F10 ICC-SC were lentivirally transduced with the pGreenFire-p53-mCMV-EF1α-Puro Transcriptional Reporter purchased as a virus (System Biosciences, Palo Alto, CA). The 0.5×10^5 2xSCS2F10 cells were plated in a 24-well plate. The next day the media were replaced with 0.5 mL media containing 5 mg/mL Polybrene, and the cells were infected with the pseudovirus. On day 3 the media were changed to Polybrene-free media, and the cells were incubated overnight. On day 4 the cells were split, incubated for additional 48 hours, and then treated with nutlin 3a (10 μmol/L) or DMSO vehicle for 3 days. The cells were clonally plated on the basis of green fluorescent protein fluorescence reporting TRP53 activity (high vs low) by fluorescence-activated cell sorting. Cell viability was quantified by MTS assay after 14 days of culturing in the absence of nutlin 3a.

Statistical Analyses

Data were expressed as mean ± standard deviation or median and interquartile range with 5th and 95th percentiles shown as appropriate. Each graph also contains an overlaid scatter plot showing all independent observations. The "n" in the figure legends refers to these independent observations. Hypothesis testing was performed by nonparametric methods including the Mann-Whitney rank sum test and the Kruskal-Wallis one-way analysis of variance (ANOVA) on ranks followed by appropriate post hoc tests (Tukey's test and Dunn's method). The *t* tests were only applied to arcsine square root transformed proportional data and when the sample size equaled 3. Proportions were analyzed by the χ^2 test. $P < .05$ was considered statistically significant. Methods used for the analysis of transcriptome data are described under "Transcriptome Data Analysis".

Methods

All authors had access to the study data and reviewed and approved the final manuscript.

Regulatory Approvals

De-identified gastric corpus tissues were collected from nondiabetic patients undergoing bariatric surgery (Institutional Review Board protocol 13-008138). Animal experiments were performed in accordance with the National Institutes of Health Guide for the Care and Use of Laboratory Animals. The protocols were approved by the Mayo Clinic Institutional Animal Care and Use Committee (A64812, A48315). Protocols for work with biohazardous agents, recombinant DNA, and synthetic nucleic acids including gene expression plasmids, reporter lentivectors, and siRNA were approved by the Mayo Clinic Institutional Biosafety Committee (Bios00000076.01). Work with these agents was performed at biocontainment level BSL2 or BSL2þ according to standard operating procedures covering personal protective equipment use, decontamination, and waste handling.

References

1. Kennedy BK, Berger SL, Brunet A, Campisi J, Cuervo AM, Epel ES, Franceschi C, Lithgow GJ, Morimoto RI, Pessin JE, Rando TA, Richardson A, Schadt EE, Wyss-Coray T, Sierra F. Geroscience: linking aging to chronic disease. Cell 2014; 159:709–713.
2. Camilleri M, Cowen T, Koch TR. Enteric neurodegeneration in ageing. Neurogastroenterol Motil 2008; 20:185–196.
3. Bhutto A, Morley JE. The clinical significance of gastrointestinal changes with aging. Curr Opin Clin Nutr Metab Care 2008;11:651–660.
4. Salles N. Is stomach spontaneously ageing? pathophysiology of the ageing stomach. Best Pract Res Clin Gastroenterol 2009;23:805–819.
5. Parker BA, Chapman IM. Food intake and ageing: the role of the gut. Mech Ageing Dev 2004;125:859–866.

6. Levine ME, Suarez JA, Brandhorst S, Balasubramanian P, Cheng CW, Madia F, Fontana L, Mirisola MG, Guevara-Aguirre J, Wan J, Passarino G, Kennedy BK, Wei M, Cohen P, Crimmins EM, Longo VD. Low protein intake is associated with a major reduction in IGF-1, cancer, and overall mortality in the 65 and younger but not older population. Cell Metab 2014; 19:407–417.
7. Sanders KM, Ward SM. Nitric oxide and its role as a non-adrenergic, non-cholinergic inhibitory neurotransmitter in the gastrointestinal tract. Br J Pharmacol 2019; 176:212–227.
8. Phillips RJ, Kieffer EJ, Powley TL. Aging of the myenteric plexus: neuronal loss is specific to cholinergic neurons. Auton Neurosci 2003;106:69–83.
9. Phillips RJ, Powley TL. Innervation of the gastrointestinal tract: patterns of aging. Auton Neurosci 2007; 136:1–19.
10. Bernard CE, Gibbons SJ, Gomez-Pinilla PJ, Lurken MS, Schmalz PF, Roeder JL, Linden D, Cima RR, Dozois EJ, Larson DW, Camilleri M, Zinsmeister AR, Pozo MJ, Hicks GA, Farrugia G. Effect of age on the enteric nervous system of the human colon. Neurogastroenterol Motil 2009;21:746–e746.
11. Izbeki F, Asuzu DT, Lorincz A, Bardsley MR, Popko LN, Choi KM, Young DL, Hayashi Y, Linden DR, Kuro-o M, Farrugia G, Ordog T. Loss of Kitlow progenitors, reduced stem cell factor and high oxidative stress underlie gastric dysfunction in progeric mice. J Physiol 2010; 588:3101–3117.
12. Asuzu DT, Hayashi Y, Izbeki F, Popko LN, Young DL, Bardsley MR, Lorincz A, Kuro OM, Linden DR, Farrugia G, Ordog T. Generalized neuromuscular hypoplasia, reduced smooth muscle myosin and altered gut motility in the klotho model of premature aging. Neurogastroenterol Motil 2011; 23:e309–e323.
13. Broad J, Kung VWS, Palmer A, Elahi S, Karami A, Darreh-Shori T, Ahmed S, Thaha MA, Carroll R, Chin-Aleong J, Martin JE, Saffrey MJ, Knowles CH, Sanger GJ. Changes in neuromuscular structure and functions of human colon during ageing are region-dependent. Gut 2019; 68:1210–1223.
14. Sanders KM, Kito Y, Hwang SJ, Ward SM. Regulation of gastrointestinal smooth muscle function by interstitial cells. Physiology (Bethesda) 2016;31:316–326.
15. Gomez-Pinilla PJ, Gibbons SJ, Sarr MG, Kendrick ML, Shen KR, Cima RR, Dozois EJ, Larson DW, Ordog T, Pozo MJ, Farrugia G. Changes in interstitial cells of cajal with age in the human stomach and colon. Neurogastroenterol Motil 2011;23:36–44.
16. Kuro-o M, Matsumura Y, Aizawa H, Kawaguchi H, Suga T, Utsugi T, Ohyama Y, Kurabayashi M, Kaname T, Kume E, Iwasaki H, Iida A, Shiraki-Iida T, Nishikawa S, Nagai R, Nabeshima YI. Mutation of the mouse klotho gene leads to a syndrome resembling ageing. Nature 1997;390:45–51.
17. van Deursen JM. The role of senescent cells in ageing. Nature 2014;509:439–446.
18. Campisi J. Aging, cellular senescence, and cancer. Annu Rev Physiol 2013;75:685–705.
19. Rossi DJ, Jamieson CH, Weissman IL. Stems cells and the pathways to aging and cancer. Cell 2008; 132:681–696.
20. Lorincz A, Redelman D, Horvath VJ, Bardsley MR, Chen H, Ordog T. Progenitors of interstitial cells of cajal in the postnatal murine stomach. Gastroenterology 2008; 134:1083–1093.
21. Bardsley MR, Horvath VJ, Asuzu DT, Lorincz A, Redelman D, Hayashi Y, Popko LN, Young DL, Lomberk GA, Urrutia RA, Farrugia G, Rubin BP, Ordog T. Kitlow stem cells cause resistance to Kit/platelet-derived growth factor alpha inhibitors in murine gastrointestinal stromal tumors. Gastroenterology 2010;139:942–952.
22. Dave M, Hayashi Y, Gajdos GB, Smyrk TC, Svingen PA, Kvasha SM, Lorincz A, Dong H, Faubion WA Jr, Ordog T. Stem cells for murine interstitial cells of cajal suppress cellular immunity and colitis via prostaglandin E2 secretion. Gastroenterology 2015;148:978–990.
23. Nusse R, Clevers H. Wnt/beta-catenin signaling, disease, and emerging therapeutic modalities. Cell 2017; 169:985–999.
24. Reya T, Duncan AW, Ailles L, Domen J, Scherer DC, Willert K, Hintz L, Nusse R, Weissman IL. A role for Wnt signalling in self-renewal of haematopoietic stem cells. Nature 2003;423:409–414.
25. Brack AS, Conboy MJ, Roy S, Lee M, Kuo CJ, Keller C, Rando TA. Increased Wnt signaling during aging alters muscle stem cell fate and increases fibrosis. Science 2007;317:807–810.
26. Castilho RM, Squarize CH, Chodosh LA, Williams BO, Gutkind JS. mTOR mediates Wnt-induced epidermal stem cell exhaustion and aging. Cell Stem Cell 2009; 5:279–289.
27. Kirstetter P, Anderson K, Porse BT, Jacobsen SE, Nerlov C. Activation of the canonical Wnt pathway leads to loss of hematopoietic stem cell repopulation and multilineage differentiation block. Nat Immunol 2006; 7:1048–1056.
28. Liu H, Fergusson MM, Castilho RM, Liu J, Cao L, Chen J, Malide D, Rovira II, Schimel D, Kuo CJ, Gutkind JS, Hwang PM, Finkel T. Augmented Wnt signaling in a mammalian model of accelerated aging. Science 2007; 317:803–806.
29. Damalas A, Ben-Ze'ev A, Simcha I, Shtutman M, Leal JF, Zhurinsky J, Geiger B, Oren M. Excess beta-catenin promotes accumulation of transcriptionally active p53. EMBO J 1999;18:3054–3063.
30. Krenning L, van den Berg J, Medema RH. Life or death after a break: what determines the choice? Mol Cell 2019;76:346–358.
31. Kastenhuber ER, Lowe SW. Putting p53 in context. Cell 2017;170:1062–1078.
32. Lorin S, Hamai A, Mehrpour M, Codogno P. Autophagy regulation and its role in cancer. Semin Cancer Biol 2013; 23:361–379.

33. Engeland K. Cell cycle arrest through indirect transcriptional repression by p53: I have a DREAM. Cell Death Differ 2018;25:114–132.
34. Gounari F, Chang R, Cowan J, Guo Z, Dose M, Gounaris E, Khazaie K. Loss of adenomatous polyposis coli gene function disrupts thymic development. Nat Immunol 2005;6:800–809.
35. Chi P, Chen Y, Zhang L, Guo X, Wongvipat J, Shamu T, Fletcher JA, Dewell S, Maki RG, Zheng D, Antonescu CR, Allis CD, Sawyers CL. ETV1 is a lineage survival factor that cooperates with KIT in gastrointestinal stromal tumours. Nature 2010;467:849–853.
36. Hayashi Y, Toyomasu Y, Saravanaperumal SA, Bardsley MR, Smestad JA, Lorincz A, Eisenman ST, Cipriani G, Nelson Holte MH, Al Khazal FJ, Syed SA, Gajdos GB, Choi KM, Stoltz GJ, Miller KE, Kendrick ML, Rubin BP, Gibbons SJ, Bharucha AE, Linden DR, Maher LJ 3rd, Farrugia G, Ordog T. Hyperglycemia increases interstitial cells of Cajal via MAPK1 and MAPK3 signaling to ETV1 and KIT, leading to rapid gastric emptying. Gastroenterology 2017;153:521–535 e520.
37. Syed SA, Hayashi Y, Lee JH, Yan H, Lorincz A, Strege PR, Gajdos GB, Milosavljevic S, Nie J, Rumessen JJ, Gibbons SJ, Horvath VJ, Bardsley MR, Redelman DD, Klein S, Saur D, Farrugia G, Zhang Z, Urrutia R, Ordog T. Ezh2-dependent epigenetic reprogramming controls a developmental switch between modes of gastric neuromuscular regulation. bioRxiv 2018. https://doi.org/10.1101/486423.
38. Lee MY, Ha SE, Park C, Park PJ, Fuchs R, Wei L, Jorgensen BG, Redelman D, Ward SM, Sanders KM, Ro S. Transcriptome of interstitial cells of Cajal reveals unique and selective gene signatures. PLoS One 2017;12:e0176031.
39. Chen H, Ordog T, Chen J, Young DL, Bardsley MR, Redelman D, Ward SM, Sanders KM. Differential gene expression in functional classes of interstitial cells of Cajal in murine small intestine. Physiol Genomics 2007;31:492–509.
40. Tang CM, Lee TE, Syed SA, Burgoyne AM, Leonard SY, Gao F, Chan JC, Shi E, Chmielecki J, Morosini D, Wang K, Ross JS, Kendrick ML, Bardsley MR, Siena M, Mao J, Harismendy O, Ordog T, Sicklick JK. Hedgehog pathway dysregulation contributes to the pathogenesis of human gastrointestinal stromal tumors via GLI-mediated activation of KIT expression. Oncotarget 2016;7:78226–78241.
41. Subramanian A, Tamayo P, Mootha VK, Mukherjee S, Ebert BL, Gillette MA, Paulovich A, Pomeroy SL, Golub TR, Lander ES, Mesirov JP. Gene set enrichment analysis: a knowledge-based approach for interpreting genome-wide expression profiles. Proc Natl Acad Sci U S A 2005;102:15545–15550.
42. Tang X, Wang Y, Fan Z, Ji G, Wang M, Lin J, Huang S, Meltzer SJ. Klotho: a tumor suppressor and modulator of the Wnt/beta-catenin pathway in human hepatocellular carcinoma. Lab Invest 2016;96:197–205.
43. Budanov AV, Karin M. p53 target genes sestrin1 and sestrin2 connect genotoxic stress and mTOR signaling. Cell 2008;134:451–460.
44. Vassilev LT, Vu BT, Graves B, Carvajal D, Podlaski F, Filipovic Z, Kong N, Kammlott U, Lukacs C, Klein C, Fotouhi N, Liu EA. In vivo activation of the p53 pathway by small-molecule antagonists of MDM2. Science 2004;303:844–848.
45. Maier B, Gluba W, Bernier B, Turner T, Mohammad K, Guise T, Sutherland A, Thorner M, Scrable H. Modulation of mammalian life span by the short isoform of p53. Genes Dev 2004;18:306–319.
46. Larsson O, Scheele C, Liang Z, Moll J, Karlsson C, Wahlestedt C. Kinetics of senescence-associated changes of gene expression in an epithelial, temperature-sensitive SV40 large T antigen model. Cancer Res 2004;64:482–489.
47. Dimri GP, Lee X, Basile G, Acosta M, Scott G, Roskelley C, Medrano EE, Linskens M, Rubelj I, Pereira-Smith O. A biomarker that identifies senescent human cells in culture and in aging skin in vivo. Proc Natl Acad Sci U S A 1995;92:9363–9367.
48. Villanueva J, Yung Y, Walker JL, Assoian RK. ERK activity and G1 phase progression: identifying dispensable versus essential activities and primary versus secondary targets. Mol Biol Cell 2007;18:1457–1463.
49. Hayashi Y, Bardsley MR, Toyomasu Y, Milosavljevic S, Gajdos GB, Choi KM, Reid-Lombardo KM, Kendrick ML, Bingener-Casey J, Tang CM, Sicklick JK, Gibbons SJ, Farrugia G, Taguchi T, Gupta A, Rubin BP, Fletcher JA, Ramachandran A, Ordog T. Platelet-derived growth factor receptor-alpha regulates proliferation of gastrointestinal stromal tumor cells with mutations in KIT by stabilizing ETV1. Gastroenterology 2015;149:420–432 e416.
50. Fox EA, Phillips RJ, Byerly MS, Baronowsky EA, Chi MM, Powley TL. Selective loss of vagal intramuscular mechanoreceptors in mice mutant for steel factor, the c-Kit receptor ligand. Anat Embryol (Berl) 2002;205:325–342.
51. Hennig GW, Brookes SJ, Costa M. Excitatory and inhibitory motor reflexes in the isolated guinea-pig stomach. J Physiol 1997;501:197–212.
52. Takahashi T, Owyang C. Characterization of vagal pathways mediating gastric accommodation reflex in rats. J Physiol 1997;504:479–488.
53. Dixit D, Zarate N, Liu LW, Boreham DR, Huizinga JD. Interstitial cells of Cajal and adaptive relaxation in the mouse stomach. Am J Physiol Gastrointest Liver Physiol 2006;291:G1129–G1136.
54. Lee KH, Li M, Michalowski AM, Zhang X, Liao H, Chen L, Xu Y, Wu X, Huang J. A genomewide study identifies the Wnt signaling pathway as a major target of p53 in murine embryonic stem cells. Proc Natl Acad Sci U S A 2010;107:69–74.
55. Oh J, Lee YD, Wagers AJ. Stem cell aging: mechanisms, regulators and therapeutic opportunities. Nat Med 2014;20:870–880.
56. Stanich JE, Gibbons SJ, Eisenman ST, Bardsley MR, Rock JR, Harfe BD, Ordog T, Farrugia G. Ano1 as a regulator of proliferation. Am J Physiol Gastrointest Liver Physiol 2011;301:G1044–G1051.
57. Hayashi Y, Asuzu DT, Gibbons SJ, Aarsvold KH, Bardsley MR, Lomberk GA, Mathison AJ, Kendrick ML, Shen KR, Taguchi T, Gupta A, Rubin BP, Fletcher JA,

Farrugia G, Urrutia RA, Ordog T. Membrane-to-nucleus signaling links insulin-like growth factor-1- and stem cell factor-activated pathways. PLoS One 2013;8:e76822.

58. Kalari KR, Nair AA, Bhavsar JD, O'Brien DR, Davila JI, Bockol MA, Nie J, Tang X, Baheti S, Doughty JB, Middha S, Sicotte H, Thompson AE, Asmann YW, Kocher JP. MAP-RSeq: Mayo analysis pipeline for RNA sequencing. BMC Bioinformatics 2014;15:224.
59. Wang L, Wang S, Li W. RSeQC: quality control of RNA-seq experiments. Bioinformatics 2012;28:2184–2185.
60. Dobin A, Davis CA, Schlesinger F, Drenkow J, Zaleski C, Jha S, Batut P, Chaisson M, Gingeras TR. STAR: ultrafast universal RNA-seq aligner. Bioinformatics 2013;29:15–21.
61. McCarthy DJ, Chen Y, Smyth GK. Differential expression analysis of multifactor RNA-Seq experiments with respect to biological variation. Nucleic Acids Res 2012;40:4288–4297.
62. Horvath VJ, Vittal H, Lorincz A, Chen H, Almeida-Porada G, Redelman D, Ordog T. Reduced stem cell factor links smooth myopathy and loss of interstitial cells of cajal in murine diabetic gastroparesis. Gastroenterology 2006;130:759–770.

Received December 20, 2019. Accepted July 30, 2020.

Correspondence

Address correspondence to: Tamas Ordog, MD, Mayo Clinic, Guggenheim 10, 200 First Street SW, Rochester, Minnesota 55906. e-mail: ordog.tamas@mayo.edu; fax: (507) 255-6318; or Yujiro Hayashi, PhD, Mayo Clinic, Guggenheim 10, 200 First Street SW, Rochester, Minnesota 55906. e-mail: hayashi.yujiro@mayo.edu; fax: (507) 255-6318.

Acknowledgments

The authors thank Merry J. Oursler, PhD (Robert and Arlene Kogod Center on Aging, Mayo Clinic, Rochester, MN) for providing stomachs from old mice. They also thank Pritha Chanana, MS (Division of Biostatistics and Informatics, Department of Health Sciences Research) for the initial bioinformatic analysis of RNA-sequencing data and Zhenqing Ye, PhD (Division of Biostatistics and Informatics, Department of Health Sciences Research) for his help with transcriptome data archiving.

CRediT Authorship Contributions

Yujiro Hayashi, PhD (Conceptualization: Equal; Formal analysis: Lead; Funding acquisition: Supporting; Investigation: Lead; Validation: Lead; Visualization: Lead; Writing – original draft: Lead; Writing – review & editing: Supporting)

David T. Asuzu, MD, PhD (Conceptualization: Equal; Formal analysis: Supporting; Funding acquisition: Supporting; Investigation: Equal; Validation: Supporting; Visualization: Supporting; Writing – review & editing: Supporting),

Michael R. Bardsley, MS (Investigation: Supporting; Writing – review & editing: Supporting)

Gabriella B. Gajdos, MS (Investigation: Supporting; Writing – review & editing: Supporting)

Sergiy M. Kvasha, PhD (Investigation: Supporting; Writing – review & editing: Supporting)

David R. Linden, PhD (Funding acquisition: Supporting; Investigation: Supporting; Methodology: Supporting; Writing – review & editing: Supporting)

Rea A. Nagy, MD (Investigation: Supporting; Writing – review & editing: Supporting)

Siva Arumugam Saravanaperumal, PhD (Investigation: Supporting; Writing – review & editing: Supporting)

Sabriya A. Syed, PhD (Investigation: Supporting; Writing – review & editing: Supporting)

Yoshitaka Toyomasu, MD, PhD (Investigation: Supporting; Writing – review & editing: Supporting)

Huihuang Yan, PhD (Formal analysis: Supporting; Writing – review & editing: Supporting)

Eduardo N. Chini, MD, PhD (Resources: Supporting; Writing – review & editing: Supporting)

Simon J. Gibbons, PhD (Resources: Supporting; Writing – review & editing: Supporting)

Todd A. Kellogg, MD (Resources: Supporting; Writing – review & editing: Supporting)

Khashayarsha Khazaie, PhD (Methodology: Supporting; Resources: Supporting; Writing – review & editing: Supporting)

Makoto Kuro-o, PhD (Methodology: Supporting; Resources: Supporting; Writing – review & editing: Supporting)

Jair Machado Espindola Netto, PhD (Resources: Supporting; Writing – review & editing: Supporting)

Mahendra Pal Singh, PhD (Resources: Supporting; Writing – review & editing: Supporting)

James G. Tidball, PhD (Resources: Supporting; Writing – review & editing: Supporting)

Michelle Wehling-Henricks, PhD (Resources: Supporting; Writing – review & editing: Supporting)

Gianrico Farrugia, MD (Funding acquisition: Supporting; Writing – review & editing: Supporting)

Tamas Ordog, MD (Conceptualization: Equal; Formal analysis: Equal; Funding acquisition: Lead; Methodology: Supporting; Project administration: Lead; Supervision: Lead; Validation: Lead; Visualization: Supporting; Writing – original draft: Supporting; Writing – review & editing: Lead)

Conflicts of interest

The authors disclose no conflicts.

Funding

Supported in part by National Institutes of Health grants R01 DK058185 (T.O.), R01 DK121766 (Y.H.), P01 DK068055 (G.F., D.R.L., T.O.), P30 DK084567 (T.O.), F31 DK089974 (D.T.A.), an American Gastroenterology Association–Allergan Foundation Pilot Research Award in Gastroparesis (Y.H.), and the Mayo Clinic Center for Individualized Medicine (T.O.). The funding agencies had no role in the study analysis or writing of the manuscript. Its contents are solely the responsibility of the authors.